

Large-Scale Syntheses of 2D Materials: Flash Joule Heating and Other Methods

Kevin M. Wyss, Duy Xuan Luong, and James M. Tour*

In the past 17 years, the larger-scale production of graphene and graphene family materials has proven difficult and costly, thus slowing wider-scale commercial applications. The quality of the graphene that is prepared on larger scales has often been poor, demonstrating a need for improved quality controls. Here, current industrial graphene synthetic and analytical methods, as well as recent academic advancements in larger-scale or sustainable synthesis of graphene, defined here as weights more than 200 mg or films larger than 200 cm², are compiled and reviewed. There is a specific emphasis on recent research in the use of flash Joule heating as a rapid, efficient, and scalable method to produce graphene and other 2D nanomaterials. Reactor design, synthetic strategies, safety considerations, feedstock selection, Raman spectroscopy, and future outlooks for flash Joule heating syntheses are presented. To conclude, the remaining challenges and opportunities in the larger-scale synthesis of graphene and a perspective on the broader use of flash Joule heating for larger-scale 2D materials synthesis are discussed.

1997^[3–5] In 1962, Hanns-Peter Boehm first generated graphene through the reduction of graphite oxide, and he showed the TEM structure of what appears to be a monolayer material.^[6] So, the field of 2D materials has existed for decades longer than many appreciate.^[7–9] Academic interest in the synthesis has dominated the field, largely out of necessity: the synthesis of graphene and related materials is arduous, finicky, and often miniscule in scale.^[10,11] Indeed, most published studies on graphene deal in amounts on the milligram or sub-milligram scale. These obtainable weights do not allow many cutting-edge applications to be readily scaled and applied to higher levels of technological readiness or commercial application without requiring significant optimization. A multitude of demonstrated and hypothesized applications of graphene exist: composites, energy

storage, lubricants, coatings, gas storage and separations, flexible electronics, displays, sensors, catalysts, and water filtration are among the most published upon (Figure 1).^[2,12–15] The possible applications of graphene depend on the physical, electronic, and optical properties of the material, which as discussed later, are determined by the quality and number of layers. Large-area monolayer graphene films are used in applications where flexibility and moderate conductivity over large areas are required, such as solar cells, electronics, and conductivity-based sensors. However, a trade-off exists between electrical conductivity and transparency based on the number of layers of graphene film present. A typical graphene monolayer has a resistance of $\approx 1000 \Omega \text{ sq}^{-1}$, with more layers necessary to achieve lower resistances. Comparatively, indium tin oxide (ITO) has a conductivity of $60\text{--}100 \Omega \text{ sq}^{-1}$. Each graphene layer adsorbs 2.5% of transmitted light at 550 nm, so if conductivities comparable to ITO are desired using graphene, transparency is sacrificed.

However, bulk graphene powders, which can be produced in much larger scales than large-area graphene films, receive significant use in materials composites, lubricants, and energy-storage materials where the sheet morphology, intrinsic strength, and high surface area can yield substantial improvements. Bulk graphene is used in these applications due to the ability to produce adequate amounts at reasonable costs. Depending on the specific design, scale, and application, both bulk graphene or graphene films can be used in electrochemical, coating, or other applications. Both graphene powders and graphene films have shown promise in many literature applications.

1. Large-Scale Graphene Synthesis


1.1. Introduction to Larger-Scale Graphene Production

Beginning with the exfoliation of graphite into graphene using repeated peeling of Scotch tape in 2004,^[1] graphene has captured interdisciplinary research interests over the past 17 years, with more than 40 peer-reviewed publications per day mentioning graphene.^[2] However, less widely known is that exfoliation of graphite to pseudo-2D platelets was published in the early 1990s, and that chemical vapor deposition (CVD) had been used to produce graphene and hexagonal boron nitride (hBN) as early as

K. M. Wyss, D. X. Luong, J. M. Tour
 Department of Chemistry
 Rice University
 6100 Main Street, Houston, TX 77005, USA
 E-mail: tour@rice.edu

J. M. Tour
 Department of Materials Science and NanoEngineering
 Rice University
 6100 Main Street, Houston, TX 77005, USA

J. M. Tour
 Smalley-Curl Institute
 NanoCarbon Center and the Welch Institute for Advanced Materials
 Rice University
 6100 Main Street, Houston, TX 77005, USA

 The ORCID identification number(s) for the author(s) of this article can be found under <https://doi.org/10.1002/adma.202106970>.

DOI: 10.1002/adma.202106970

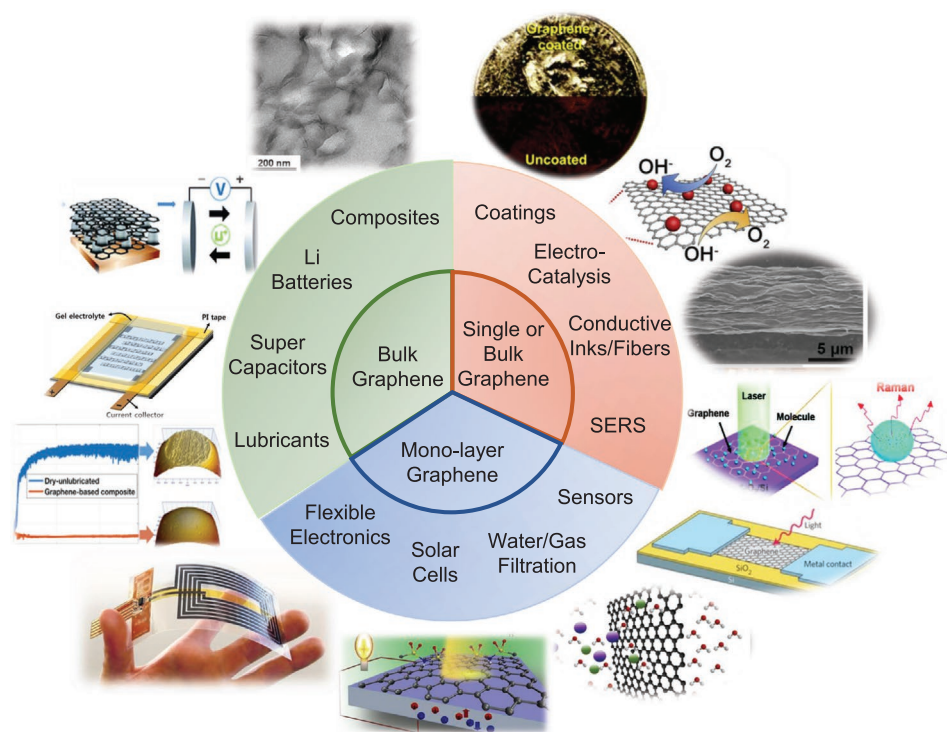


Figure 1. A diagram displaying various graphene products and some of their eventual applications. In clockwise order starting with “Coatings”: Reproduced with permission.^[38] Copyright 2011, American Chemical Society. Reproduced with permission.^[39] Copyright 2018, Elsevier. Reproduced with permission.^[40] Copyright 2015, Elsevier. Reproduced with permission.^[41] Copyright 2010, American Chemical Society. Reproduced with permission.^[42] Copyright 2010, Springer Nature. Reproduced with permission.^[43] Copyright 2021, Elsevier. Reproduced with permission.^[44] Copyright 2012, American Chemical Society. Reproduced with permission.^[45] Copyright 2018, Elsevier. Reproduced with permission.^[46] Copyright 2017, Elsevier. Reproduced with permission.^[47] Copyright 2016, Elsevier. Reproduced with permission.^[48] Copyright 2011, Royal Society of Chemistry. Reproduced with permission.^[49] Copyright 2013, Elsevier.

Many reviews exist on the desirable properties and possible applications of graphene,^[16–19] so the goal of this review is to highlight work being carried out to produce and apply larger-scale quantities of graphene materials, defined here as weights more than 200 mg or films larger than 200 cm². This scale is selected as the lower cutoff for this review since it suggests that through automation or leverage of reactors in parallel, along with process optimization, the technique might result in scales necessary for commercial or industrial study and use. Further, manuscripts published regarding production of graphene on a few-milligram or few-centimeter scale, using long reaction times or many steps, are excluded from consideration here. While those papers are noteworthy, work to translate from the bench-top to proof-of-concept scale levels of technological readiness is not usually realized. Comparison of production rates could be a valid metric, but as discussed later in this review, disclosure of production rates remains lacking in most academic graphene synthesis manuscripts. Larger-scale methods are of interest since they are essential to realizing commercial applications.

Graphene is defined stringently as “a single layer of carbon atoms, with each atom bound to three neighbors in a honeycomb structure” by the International Organization for Standards (ISO) as of 2017, but a significant variety of terminology is still employed academically and industrially.^[20] Others have suggested that 10 or fewer layers to still be considered graphene

since at <10 layers the optical properties of AB-stacked graphene are dissimilar to graphite, but this will be discussed further in Section 2.5. Several academic articles refer to graphene oxide materials or surface-modified graphene oxides as “graphene”, and terms like “pristine graphene” can be misleading. Single, bi-, and trilayer graphene are self-explanatory, while few-layer graphene is defined by ISO as consisting of 3–10 graphene layers, with no requirements as to how these layers are ordered. Graphene nanoplatelets are poorly defined and the term is widely used throughout literature. While the 2017 ISO directive has proven helpful in terminology, assignments of purity and analytical standards remain elusive.^[21]

Strict definitions can break down when studying larger-scale graphene. 2D monolayer graphene is only ever isolated in select laboratory conditions as synthesized by CVD. Any larger-scale production of graphene, especially those producing a dry powder form, will appear in aggregates of sheets, but the important distinction comes from the stacking arrangement and a number of layers. It is documented that graphite-like optical and electronic properties ensue when >9 layers are AB-stacked, hence this being the distinction between “few-layer graphene” and graphite.^[22] However, this border between 2D graphene properties and 3D graphite properties depends on whether the layers are randomly oriented with respect to one another, termed “misoriented”, “twisted”, “weakly coupled”, or “turbostratic”. The importance of this rotational disorder is

that it allows the individual graphene layers to retain several 2D properties.^[23] Hence, even when many hundreds of graphene layers are stacked, if the rotational disorder is present, the 2D definition of graphene is maintained when studied by optical and electronic means.^[24] A well-studied property to compare between graphene and graphite is the electronic properties, specifically electron mobility. Graphene, a 2D and conductive material, is highly anisotropic in electron mobility, allowing x - y motion but significantly less mobility in the z -axis.^[25] Turbostratic graphene adds to this anisotropy, and even when multiple layers are stacked, the z -axis conductivity is observed to be many orders of magnitude less than the in-plane conductivity, and turbostratic graphene remains a zero-bandgap semiconductor.^[26] However, since graphene layers are AB stacked to form graphite, the coupling of layers creates alternative energy levels at the K wave vector, inducing a bandgap.

Some researchers highlight the cost and difficulty of graphene production, arguing that the "wonder material" is far from being widely implemented.^[27] Further, some think that graphene will take decades to live up to the expectations surrounding it, such as revolutionizing manufacturing processes and improving the performance of everyday objects.^[28] We intend to convey herein that commercial and industrial-scale synthesis is already taking place, and larger-scale applications are following close behind.^[29] Flash Joule heating (FJH) is one of the most promising methods of larger-scale graphene synthesis, being highly efficient and requiring only simple input materials.^[30] The growing body of literature pertaining to FJH is discussed and contrasted with other industrial and academic methods of graphene production, and a perspective for future larger-scale and even bulk graphene development is provided.^[31–37]

1.2. Current Industrial Graphene Production Methods and Uses

Graphene production can be broadly classified into two different methodologies: the top-down and bottom-up strategies.^[50] The name of each method acknowledges whether the carbon atoms had their hexagonal molecular arrangement before the synthesis began. The bottom-up method is exemplified using chemical vapor deposition (CVD), in which CH_4 , C_2H_4 , or other simple hydrocarbons are catalytically decomposed to form graphene films on Ni, Cu, or other metal surfaces.^[51] Thus, the films are grown from the bottom (individual carbon atoms) up to graphene sheets, adding one or a few atoms at a time to the graphene crystal. Conversely, the top-down method is exemplified by the exfoliation of graphite to form graphene sheets. Here, the graphene sheets are already fully formed and are merely separated physically or chemically, from the top (already formed sheets) down to the individual or a few graphene layers.

In the larger-scale synthesis of graphene, the top-down approach is almost singularly used industrially.^[52] For industrial applications of graphene in coatings or composites, typically kilograms are required for prototype applications alone, either in powder or suspension form. For applications requiring continuous and large graphene films, such as in sensors or solar cells, bottom-up CVD synthesis is generally used, but hun-

dreds of films with high reproducibility might be required in product prototyping. It becomes readily apparent that at a cost of \$50 000–200 000 ton^{-1} for graphene powders and \$45 000–\$100 000 m^{-2} of graphene film, industrial production methods and costs are restraining graphene utility.^[53] Market research suggests that there are currently more than 800 companies producing various graphene products including graphene-enhanced composite materials, and ≈ 300 producing graphene powders.^[54] Approximately 75% of the world's graphite supply is controlled by China, and most worldwide graphene-based patents also reside in China.^[55] Notably, the European Union Graphene Flagship has pledged 1 billion euros to graphene development over 10 years.^[56] Total production of graphene and graphene nanoplatelets is currently estimated to reach 3800 ton year^{-1} , a miniscule amount when compared to other materials.^[57]

Current methods of industrial graphene powder production revolve around the physical and chemical exfoliation of graphite. Graphite is relatively inexpensive (\$1000–3000 ton^{-1}) and abundant, whereas battery-grade graphite can be \$20 000 ton^{-1} . High quality and purity are required for graphene synthesis since top-down methods rely on the graphene sheets already present in the graphite feedstock. Graphene layers are stacked in an alternating AB manner to form graphite, overlapping electron-rich areas with electron-poor areas in the neighboring sheets.^[58] These electrostatic interactions, occurring millions of times per sheet, require large energy inputs to accomplish exfoliation. The separation energy is industrially introduced using sonication, shear mixing, or ball milling, in addition to coupling with solvent or surfactant systems that reduce the interfacial energies or attractive forces between graphene sheets.^[59] Following this physical exfoliation, the graphene sheets are then segregated by density and dispersed in solution, with centrifugation commonly being used to separate exfoliated graphene from remaining graphite.^[60]

Chemical exfoliation is another common top-down method to form graphene via graphene oxide, in which strong oxidizing agents functionalize the surface of the graphite, changing the electronic structure and thus removing one or a few layers at a time.^[61,62] This functionalized single- or few-layer graphene oxide can then be purified or separated through centrifugation or filtration. However, to arrive back at the sp^2 -hybridization of graphene, the oxygen functionalities must be removed through reduction. This reduction, also known as deoxygenation, is generally carried out industrially either chemically by strong reducing agents such as hydrazine or thermally through heating under an inert atmosphere.^[63] This reduced graphene oxide is generally a lower quality product since the strong oxidation and reduction processes induce defects, and oxygen functionalities remain, lowering the conductivity of the product and decreasing the tensile strength. Due to the toxic chemical waste streams and high water demands required by Hummers' type methods, as well as poorer structure, few industrial entities produce larger-scale graphene using this method, however, it may be considered more readily scalable compared to sonication.^[64] A lack of consensus remains on what to term the product resulting from the chemical oxidation and reduction of exfoliate graphite into a graphene-like material. Some manufacturers and researchers term this reduced graphene oxide, while others refer to it somewhat misleadingly as "graphene".

Standardization and further research remain to be carried out on this topic, but reduced graphene oxide shows promise, and sometimes can outperform more pristine graphene in select applications as the oxygen functionalities increase dispersibility in polar solvent systems.^[65]

With industrial chemical and physical exfoliation methods, many obstacles still exist. Chiefly, the energy input required to exfoliate the graphite to form graphene can result in the fracturing of sheets and induction of defects within the graphene product. These defects and smaller sheet sizes can negatively impact the conductivity and tensile strength of the product, making it less favorable in demanding applications. A dilemma exists, however, in that energy is required to exfoliate fully to mono- or few-layer graphene, but this same exfoliating energy results in a lower quality product. Another major drawback of top-down graphene production lies in the excruciatingly low solubility and stability of graphene solutions. Concentrations of 1 mg mL⁻¹, or ≈0.1 wt%, are difficult to reach even in favorable solvents such as dimethylformamide (DMF) and *N*-methyl-2-pyrrolidone (NMP), or they require the addition of surfactants to aqueous solutions.^[66] Further, if the solvent is removed to ship the product as graphene powder, re-aggregation of the graphene sheets can occur, forming lower utility few-layer graphene or graphene nanoplatelets. Shipping of these solutions thus requires many folds more energy than if the graphene powder could be shipped innately. Further, the large amounts of solvent or surfactant needed to produce kilogram-scales of graphene through chemical or physical exfoliation are resource intensive and can create large amounts of chemical waste.

The industrial production of graphene was recently studied, examining 60 commercial graphene producers.^[67] It was determined that the majority of the 60 companies produce less than 10% truly single-layer graphene in their commercial products. Further, none of the companies produced a single-layer yield greater than 50% once the graphene is dispersed in solvent and spin coated on silicon oxide wafers. Even more worrisome than the number of layers is that most graphene products displayed an elemental purity of less than 90% carbon. Raman spectroscopy was carried out, but unfortunately, these differences between the 60 companies were not discussed. The Raman spectra could be used to bolster the assertion that the graphene companies are producing graphite nanoplatelets rather than single- or few-layer graphene. The authors did not evaluate bottom-up graphene manufacturers.

The most common route to form graphene films is through bottom-up CVD synthesis onto various, often pristine metallic, substrates. Plasma cleaning and high-purity copper or nickel films are often needed to achieve high quality and reproducible graphene films. Following the deposition of carbon and graphene formation on the surface, the metal is typically etched away with acid, and the graphene film is transferred to the substrate of interest for shipping or application. Significant improvements to both throughput and size have occurred in the past decade, with Samsung Technology investing in research and achieving high quality 76 cm (diagonally) films;^[68] however, most current industrial companies sell much smaller films, between 1 and 1000 cm², often shipped on polymer or silicon substrate.^[69] Advertised annual production capabilities range from 100 000 to 1 000 000 m².^[57] Aixtron recently

released a turn-key roll-to-roll system for larger-scale bottom-up synthesis, advertising 20 000 m² per year capabilities per unit.^[70] A general roll-to-roll CVD synthetic scheme is shown in Figure 2a,b. Batch wafer-scale production is another widely used industrial CVD method, as shown in Figure 2c–e. Copper foils account for >50% of the cost to synthesize graphene films, and etching is a chemically intensive and wasteful method, but few industrially viable alternatives exist.^[69]

Another well-established bottom-up method is to synthesize graphene materials is through laser induction. Laser-induced graphene (LIG) was discovered in 2014 by Lin et al. and represents a cost-effective and rapid method to pattern highly conductive graphene foams onto polymeric or other carbon-containing materials.^[71] LIG represented one of the first single-step, accessible, and scalable methods to pattern graphene materials, and it is enjoying extensive academic use as well as commercial applications in a growing number of areas. LIGC Application Ltd. is commercializing portable LIG air filter units as their first commercial product.^[72] Several reviews exist on the implementation and scalability of LIG, so this will not be extensively discussed here.^[73,74] However, recent work to produce laminated LIG composites in roll-to-roll high-throughput manners and patterning of high-resolution LIG onto photoresist materials indicate that flexible electronics and on-chip applications may soon see industrialization.^[75,76]

As graphene production capabilities have increased, commercial applications are finally being realized now that the cost of entry has been reduced. Due to the confidential nature of industrial research and development, it is impossible to know what the future graphene market demand will be. However, a handful of truly larger-scale industrial operations are already disclosing their use of bulk graphene products. One of the exemplary applications is the use of larger-scale graphene in late-model automobiles being produced by Ford Motor Company, which began in 2018. Graphene supplied by XG Sciences is used in foam cushions and under-hood insulation in all Ford models since February 2020.^[77] Bulk graphene destined for use in composites is generally synthesized through liquid-phase exfoliation of graphite, as shown in Figure 2f. This work began in 2014, interacting closely with the producers on a laboratory scale, before entering prototype scale applications a few years later. The polyurethane foam present in the engine compartments was enhanced with graphene to improve noise reduction, heat dissipation, and durability while lowering weight. This commercial application is an excellent example of the graphene industry as a whole: years of optimization in the laboratory and prototyping stages to arrive at a product that is cost effective and requiring only small assembly line level changes. Yet, this work pays off in producing greatly improved products at only a 0.35 wt% graphene additive level. Further applications, including the addition of graphene into bumpers through extrusion molding and coatings, are also being explored, and may soon debut to the market. Another major bulk use of graphene that has already been realized industrially is its use in lithium rechargeable batteries and supercapacitors. Companies such as US-based Real Graphene, Australian-based Graphene Manufacturing Group, and Chinese-based GAC New Energy are already mass-producing graphene battery-based products which are available on the market.^[78–80] Further, companies such as

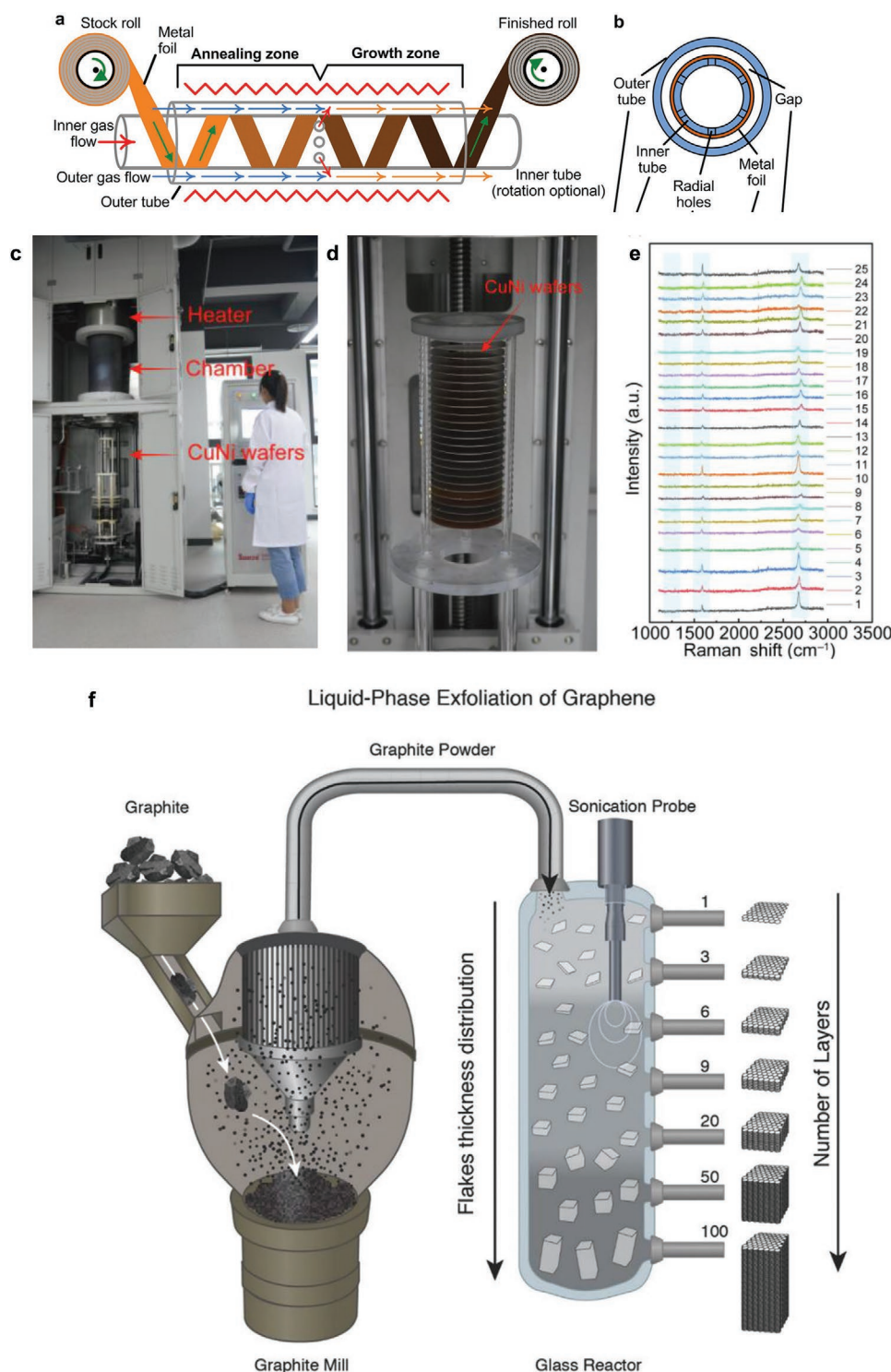


Figure 2. a,b) Industrial-scale graphene production through a roll-to-roll CVD on copper film method. c–e) Industrial-scale batch production of graphene on CuNi wafer substrate. f) Industrial-scale graphene production through a sonication-based liquid-phase exfoliation method. a,b) Reproduced under the terms of the CC-BY Creative Commons Attribution 4.0 International license (<https://creativecommons.org/licenses/by/4.0>).^[87] Copyright 2015, The Authors, published by Springer Nature. c–e) Reproduced with permission.^[88] Copyright 2019, Elsevier. f) Reproduced with permission.^[67] Copyright 2018, Wiley-VCH.

Chongqing Graphene Technologies and Wuxi Graphene Films are already producing terminal products such as flexible devices and touch screens.^[81,82] Several major companies such as Tesla,

Samsung, and Dupont are studying graphene in the coating, battery, and flexible electronics applications.^[83–85] Collaborations at the interface of academic, start-up level companies, and

major corporations are growing, especially as governments allocate large amounts of funding to graphene research.

From a survey of the current graphene production and consumption industry, significant progress in production capability has been achieved over the past decade. However, the highly variable properties of commercially available graphene would likely benefit from stronger characterization standards and closer interaction between end-users and producers, to specifically tailor the material for the desired application. Many previous manuscripts, reviews, and perspectives have bemoaned the need for graphene grades through an international standardizing body, and we agree that this will be essential to further standardize research and prevent the graphene production industry from being haphazard materials sales. Lastly, few technoeconomic assessments or life cycle assessments exist on the larger-scale production of graphene, which are essential to better understand the environmental impact of this new material on the ecosystem.^[86] As green-chemistry regulations increase, increased efficiency to lower greenhouse gas emissions and minimization of hazardous waste and by-product streams will be essential for long-term sustainability in the graphene industry.

1.3. Current Academic Advancements in Bulk Top-Down Graphene Production

As discussed above, significant shortcomings still exist in the industrial-scale production of both graphene powders/solutions and graphene films, and much academic research has been devoted to ameliorating these problems. As in its initial discovery by Novoselov and Geim, most of the larger-scale graphene synthesis has centered around the top-down production through chemical or physical exfoliation. Academic work has largely remained focused on this process as well, chasing methods that result in less energy and time being used to exfoliate, producing higher-quality graphene (fewer layers and fewer defects), or using a less accompanying solvent or chemicals during production.

One relatively recent, yet truly advancing development was work from the Coleman group to show that shear mixing can be used as a scalable method to arrive at few-layer graphene nanosheets.^[89] In this extremely detail-oriented manuscript, the authors work to optimize many shear mixing parameters in NMP, aqueous surfactant solution (sodium cholate), and poly(vinyl alcohol) (PVA) solutions, to exfoliate large amounts of high-quality graphene nanosheets with average thicknesses of 5 nm. Much characterization such as average Raman spectra and 100+ sheet histograms are presented. Calculations and discussions on exfoliation and laminar flow are also presented with new models for the rheology and shear-induced interlayer sliding. Mechanistic arguments discussing the turbulence, solvent limitations, sheet sizes, and comparisons with sonication and the greater literature body are also given. Process generality to other 2D materials such as hBN was also shown, and production rates of graphene nanosheets as high as 5.3 g h⁻¹ are obtained, with a scale up to 300 L being successfully demonstrated. The authors use extensive modeling to estimate that at a 10 000 L scale, production rates exceeding 100 g h⁻¹ might

be possible. This academic study of larger-scale graphene synthesis with its characterization methods and discussions form an excellent framework for the standards that should be presented. Discussions of yield, scale-up, and optimization also serve as a quality blueprint for other larger-scale exfoliation methods. Prompted by the Coleman approach, many other methods have been discovered. For example, Kaplan's group used naturally occurring and easily isolated silk nanofibers as a surfactant during kitchen blender shear mixing.^[90] They were able to achieve graphene concentrations of 8.6 mg mL⁻¹ with 30% yields of few-layer graphene with good lateral size. Advances such as these allow for less solvent and parent graphite to be used during physical exfoliation processes, as well as less energy compared to sonication.

Significant work has also been devoted to the calculation and optimization of hydrodynamic effects that occur during the successful exfoliation of graphene. As mentioned previously, Coleman and co-workers have proposed multiple theories, and the Taylor–Couette flow system is used largely in the field. One recent example used real-time in situ optical microscopy and high-speed cameras with image processing scripts to track the graphite precursor and the exfoliated sheets to study the speed, agglomeration, and live production rates during shear exfoliation.^[91] The production of few-layer graphene mechanistically depends on local strain rate distribution and graphite residence time, providing critical exfoliation criteria for scaling. High-resolution 3D flow simulations were also carried out to further study how strain rate and topology impact exfoliation. The study concluded by applying the gained fundamental knowledge to tailor product distributions through real-time feedback and control of shear rates and disclosing essential considerations for shear exfoliation scale-up. This study is an excellent example of how fundamental study can culminate and be applied to larger-scale graphene production questions, and reward both academic and industrial realms.

A recent exciting development to the field of physical exfoliation was the appearance of “multi-roll milling”, billed as an alternative to ball milling. Whereas ball milling is stochastic in nature and often results in decreases in graphene sheet size and quality due to the collisions, Yousef et al. constructed a belt-driven instrument that uses a set of gears to apply uniform shear rates, like existing industrial multi-roller wet-milling units used for malting corn.^[92] The graphite is in a DMF suspension before going into the unit, and brief sonication and centrifugation are used after processing to remove unexfoliated graphite prior to drying. This affords a graphene nanoplatelet powder in batches of more than 100 g. The Raman microscopy showed low defects and some presence of single-sheet graphene, but no average Raman spectra were presented. Further, no atomic force microscopy (AFM) analyses were shown, but yield analysis suggests a 91% efficiency and high recovery and re-use of DMF. Further advances of this technique, possibly resulting in few-layer graphene production, will be interesting.

Significant advances in ultrasonication techniques have also taken place in the past few years. One of the areas receiving the most attention is the use of supercritical CO₂ to assist the exfoliation.^[93] Supercritical CO₂ is able to penetrate the sheet structure and exfoliate by cavitation and it removes the need to use a surfactant during sonication. It also shortens the duration of

sonication, reducing defect formation and thereby maintaining elemental purity. AFM analysis showed that 93% of the formed graphene was <4 layers thick, and 58% yields from graphite were observed. Supercritical CO₂ is already widely used industrially, paving the way for possible scaled-up use of this high-efficiency industrial-scale synthesis method. A similar approach can be seen across literature using intercalating agents during sonication.

Newer methods have eliminated the need for sonication. One example used Br₂ as an intercalating agent followed by 10 s microwave irradiation of the dried intercalated graphite.^[94] No rinsing was reported, and Raman characterization of the powder showed production of few-layer graphene. AFM analysis showed almost exclusively single or bilayer product with lateral sizes up to 5 μm . Low defect concentrations, short processing times, and decreased use of solvent are promising advances, with demonstrated use in graphene film fabrication and application in catalytic water splitting.

Another approach gaining popularity and seeing increased scalability is the use of intercalation followed by electrochemically assisted exfoliation. Electrochemical exfoliation of graphite to graphene has seen significant research activity. A voltage is applied in a setup similar to an electrolytic cell. Graphite is used as one of the electrodes, and water is generally used as the solvent. Small amounts of ionic electrolyte are often used, which are drawn between the sheets due to the applied voltage. These ions, with accompanying water molecules, can intercalate between the graphene sheets, where the applied voltage results in the formation of oxygen gas, breaking the interactions and exfoliating graphene. This exfoliation results in the graphite monolith electrode gradually being consumed and the formation of few-layer graphene or graphite nanoplatelets. Since no sonication is used, very low defect concentrations can be obtained, however cavitation can still produce defects. One common shortcoming with this method is that once few-layer graphene or graphite nanoplatelets are removed from the monolith, they are no longer part of the electrolytic circuit, and thus they experience no further exfoliation. Hence large distributions in product thickness occur.

Recently, Zhang and Xu reported production rates as high as 25 g h⁻¹ for few-layer graphene (70% being 1–3 layer) with a 0.08 D/G ratio and high conductivities and very low defect densities using electrochemically assisted exfoliation.^[95] Raman spectroscopy, and namely the ratio of 2D/G and D/G peaks allow analysis of the quality and physical arrangement of graphene sheets, which we discuss further in Section 2.5. This was accomplished through the judicious use of alkylammonium perchlorate salts as ionic intercalating agents, and an applied voltage of 5 V. High concentration graphene inks with high conductivities were then demonstrated. High-temperature exfoliation following intercalation in an inert tube furnace at 800 °C is required to arrive at the final graphene product. The larger scale, yield, and purity of these electrochemically and intercalating-agent-assisted methods are promising.

Similarly, deep eutectic solvent systems (multiple dissolved salts, resulting in multiple ionic species) are being studied as intercalating agents for electrochemical exfoliation. One example of this method achieved gram-scale one-pot exfoliation of graphite electrodes to few-layer graphene using deep eutectic

solvents and a 7 V electrochemical potential.^[96] The graphene had a moderate defect concentration, and some elemental contamination was reported even after rinsing. Yields and scale-up considerations such as energy consumption per unit product were discussed, which are essential for further study of this possible bulk production method.

Interestingly, a nonelectrified electrochemical method of exfoliation was reported recently, leveraging the electrochemical reaction of lithium particles with graphite so that the process consumes no external electricity.^[97] Up to ≈ 16 g of graphene nanosheets can be produced in ≈ 8 h from 20 g of graphite, showing good elemental purity and few-layered thickness. No AFM analysis was conducted to further understand the size or thickness distribution, but the application of the graphene nanosheets was demonstrated in lithium-ion batteries, showing increased capacities compared to chemically exfoliated and reduced graphene oxide.

A recent approach involves the solvent-free exfoliation of graphite. Excellent work by Islam et al. used commercially available plasma spraying to exfoliate graphite using just argon and hydrogen gases (Figure 3).^[98] Stringent characterization was carried out, showing 95% carbon content, 95% sp² character, and an average thickness of 1 nm with almost no discernable D peak character. Most impressively, production rates of up to 48 g h⁻¹ are reported with no use of solvent. Mechanistically, they assert that the exfoliation results from thermal shock on the graphite by the plasma, followed by shearing in the laminar and turbulent plasma flow regions. Temperature, flow rates, and graphite particle velocity were optimized, and material cost of \$1.12 g⁻¹ was estimated with demonstrated batch-to-batch reproducibility. The authors continued to probe the physical and electronic properties of the graphene sheets as well as lubricity, film transmittance, and cyclic voltammetry demonstrating high-quality sheets. This study marks the highest published production rate for the solvent-free larger-scale synthesis of very high-quality graphene powders, and future developments using this technique will be interesting to follow.

Another solvent-free top-down synthetic method includes the use of arc-discharge methods, which will be discussed in more detail in Section 2.1. However, academic research has leveraged the technique using commercial arc welding machines to discharge high currents (≈ 150 A) through graphite electrodes kept 1 mm apart, while under N₂/H₂ gas flow.^[99] The precise mechanism is still debated, but one explanation is that exfoliation results from the high-temperature plasmas generated between the graphite electrodes colliding and intercalating between the graphene sheets, expanding, and depositing the graphene product on the side-wall of the container. Significant amounts of the graphite are converted to other amorphous carbons and must be removed through annealing at 400 °C, but few-layer graphene production rates above 12 g h⁻¹ are still able to be achieved. The graphene was then characterized using TEM and AFM, showing sub-micrometer-sized sheets and few-layer thickness, while XPS observed excellent carbon purity. However, some defects were present by Raman spectroscopy. Application of the product was demonstrated in lithium-ion batteries which showed a reversible capacity of 390 mAh g⁻¹ after 300 cycles.

These highlighted solvent-free methods are promising since they significantly lower the overall process mass intensity,

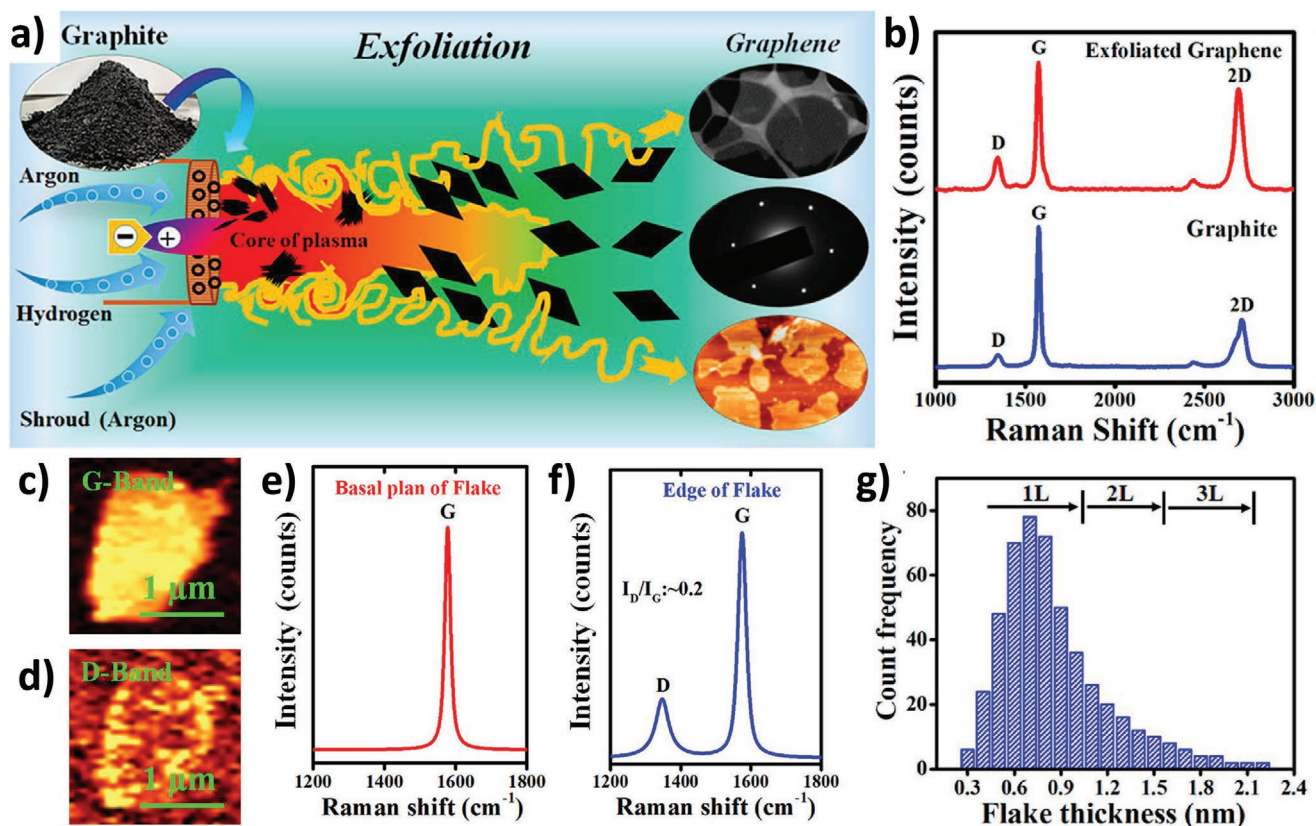


Figure 3. a) A schematic showing the plasma spray exfoliation of graphite. b) Representative Raman spectra of the produced graphene, c,d) Raman maps of a single sheet of graphene showing the intensity of the G and D bands with e,f) representative Raman spectra for the Basal plane and edge of the flake. g) A histogram showing the AFM determined thickness of 400 graphene flakes. a–f) Reproduced with permission.^[98] Copyright 2021, American Chemical Society.

although large amounts of high-purity gases are still required. Process mass intensity is a mass-based metric to evaluate the sustainability of an individual or sequence of chemical reactions, calculating the ratio of reactant mass required to produce a mass of isolated product. Production of high-quality dry graphene powder can drastically lower shipping costs as compared to shipping dilute (<1% wt) graphene solutions, as well as adding more choices for end users to employ the graphene in their specific applications.

1.4. Current Academic Advancements in Larger-Scale Bottom-Up Graphene Production

In the field of bottom-up graphene synthesis, academic research groups have focused on many areas to increase the overall production rate and quality, while lowering the cost of graphene film production. Increases in overall film production rate have been realized most strikingly in the continued development of roll-to-roll methods, reaching 25 cm min⁻¹.^[87,100] A typical roll-to-roll system will use Cu foil that first travels through an annealing zone to clean the surface and increase the crystallinity of the substrate, before traveling to a growth zone where graphene is synthesized on the surface of the foil. Use of lower temperatures or shorter heating durations has also shown

promise to increase the overall production rate, while computational modeling of furnaces and deposition mechanisms has allowed more efficient design and packing of wafers in batch CVD reactions. Careful engineering of substrate materials has also improved the rate of graphene formation, and Cu–Ni alloys were shown to accelerate the rate of graphene film synthesis.^[101] Deng et al. extended this concept through the use of a single-crystal Cu₉₀Ni₁₀(111) growth surface.^[88] The substrate wafer was manufactured through a somewhat arduous spin-coating and recrystallization method but resulted in the growth of 10 cm single-crystal graphene films in 10 min, or 500× faster than growth on pure Cu(111) faces.

In the past several years, significant effort has been devoted to reducing the number of crystal domains or grain boundaries that result from a given CVD synthesis. These grain boundaries can affect the mechanical, chemical, and electronic properties of the film, making single-crystal graphene films extremely desirable. A few key strategies have emerged in this field, such as minimizing or passivating substrate crystal domains thus reducing the active nucleation sites, locally feeding the precursor hydrocarbon so adequate nucleation concentrations are present at a few or single nucleation sites, or operating the entire reaction chamber at lower hydrocarbon concentrations to slow overall nucleation while naturally resulting in slower overall growth.^[102,103] Synthesis of single-crystal graphene with

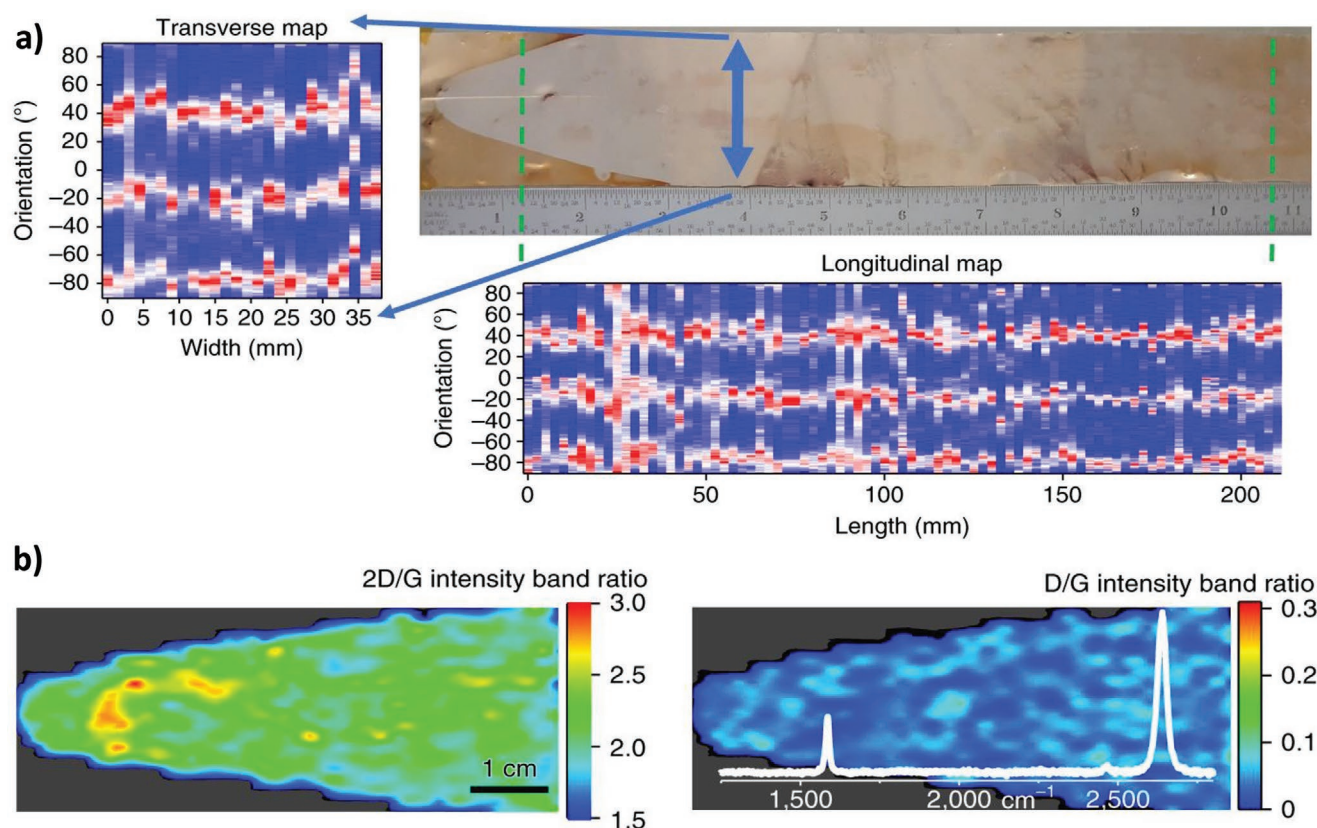


Figure 4. An example of 32 cm × 5 cm single-crystal graphene film synthesis using roll-to-roll compatible methods demonstrating a) orientation of hexagonally etched holes to confirm crystal orientation; b) large-area Raman mapping showing high-quality single-layer graphene. a,b) Reproduced with permission.^[104] Copyright 2018, The Authors, published by Springer Nature.

acceptable production rates and in a method compatible with roll-to-roll scale-up was demonstrated by Vlassioulak et al.^[104] They grew a single-crystal graphene film that are more than 30 cm long, on a polycrystalline Cu/Ni substrate with excellent quality, through localized feeding of methane. As shown in **Figure 4**, large graphene sheets can be synthesized, with the single crystallinity being demonstrated through microscopy image analysis of etched hexagonal holes in the sheet. Extremely low defect concentrations and the expected 2D/G ratio of 2–3 are observed. This technique has inspired several other developments, including the application of these methods in hBN and other inorganic 2D materials synthesis.

Improved removal of synthesized graphene films from the foil substrates has also been a focal point of academic research since current etching methods are both time-intensive and wasteful. Further, many transfer methods result in damaging, folding, or cracking of the graphene sheet, most easily measured by an increase in sheet resistance. Several transfer strategies exist, however, "bubble-assisted" and roll-to-roll transfer methods generally show the most promise for larger-scale scale and higher efficiency. Some residues may be left on the graphene sheets during polymer or other assisted transfer methods, which may result in a decreased conductivity. Bubble-assisted transfer methods have been known for more than a decade and allow the reuse of growth substrate. This results from the chemical or electrochemical formation of gas between

the graphene and growth substrate, thus removing the graphene layer. Significant improvements in scale allow for at least seven cycles of growth substrate reuse.^[105] One especially exciting academic development was the combined use of roll-to-roll lamination and scalability with bubble transfer demonstrated by Hempel and co-workers.^[106] This work demonstrated acceptable sheet resistances, as well as allowing for graphene–graphene or graphene–hBN stacking by roll-to-roll methods. This same technique was further advanced by the same group two years later to add a layer of parylene prior to the roll-to-roll bubble assisted transfer, resulting in very low sheet resistances below 300 Ω sq^{−1}.^[107]

Another approach to bypass the transfer step is to grow the graphene film directly on the end-application substrate, such as a flexible electronic platform, however this requires CVD temperatures to be far lower. One excellent example of this came when Park et al. reported that the addition of a nano-thin Ti layer atop glass or polymer substrates allows for CVD graphene synthesis to proceed at a substrate temperature of 150 °C and still produce high-quality graphene films.^[108] Although higher temperatures are still used in other regions of the CVD, the ability to maintain the growth substrate at such low temperatures allows for direct growth of graphene on the desired device with no observed impact resulting from the Ti layer.

Recent academic study into the synthesis of larger-scale graphene from a bottom-up strategy has also blossomed. One

exciting example of this was simple NaCl crystals in conjunction with plasma and pyridine precursor by CVD to synthesize nitrogen-doped graphene powders that could be dispersed to few-layer graphene.^[109] They made more than 1.6 g, however no yield per batch was reported. Another report of the bottom-up, larger-scale synthesis of graphene powder was reported, where MgO and Mg powder were used to generate a self-propagating high-temperature synthesis, which then converted CO₂ into graphene.^[110] Batch sizes up to 5.05 g of graphene powder were reported, however, overall low 2D peak intensities and high defect concentrations were observed by Raman analysis. This low graphene crystallinity increased the surface area and made it an ideal candidate for use in high-capacity supercapacitors, which retained 90% of the capacitance after 10⁶ cycles. This example demonstrates that high graphene quality is not always necessary, or even best, for some applications, emphasizing the need for interface between graphene manufacturers and end-product users. Another recent larger-scale bottom-up synthetic method used microwave plasma and ethanol precursor to form high-quality graphene powder at a rate of 1.33 mg min⁻¹.^[111] Characterization showed low defects, and an average 2D/G ratio of 1.5 and layers of 2–7 sheets. Drawbacks for this method include large amounts of Ar and ethanol used for the relatively small amounts of graphene formed.

Another study demonstrated that the detonation of acetylene with varying ratios of O₂ gas resulted in the synthesis of graphene.^[112] During detonation, temperatures of 4000 K and high pressures are reached, which the authors assert as a rationale for graphene being formed rather than amorphous soot. Raman spectroscopy and TEM imaging were used to characterize the graphene powder, and discussion of industrial scale-up was presented, asserting that production rates of 300 g h⁻¹ could be realized. No applications of the graphene produced by this simple, rapid, and solvent-free bottom-up synthesis method were presented.

1.5. Current Academic Advancements in Sustainable Larger-Scale Graphene Production

Aside from improvements in production scale and production rate, improvements in sustainability and process mass intensity are also necessary for the bulk graphene industry to excel. Alternative feedstock targets to combat the high-purity gases in CVD synthesis, large amounts of solvent needed in sonication exfoliation, or harsh oxidizing and reducing agents required in chemical exfoliation, have received much recent research attention.

As discussed above, some success has been achieved in lowering the temperatures required for both CVD substrate annealing and growth with many works now reporting temperatures below 600 °C. Temperatures of 300 °C using benzene as a carbon source were reported by Jang et al.,^[113] and temperatures of 100 °C and below were achieved by Fujita et al. through the use of gallium catalysts and island nucleation.^[114] However, high-temperature annealing of the substrate is still required for many of these methods, so overall lowering of the energy and heat demands for the entire CVD process remains a necessary area of study. Another exciting area of research in sustainable

bottom-up synthesis is attempts to remove the need to use high-purity carbon precursor gases that can be costly and less sustainable. One recent publication used the hydrocarbon-rich gases resulting from the pyrolysis of waste sawdust as a more environmentally friendly carbon source in CVD formation of high-purity graphene foam.^[115] Ar carrier gas was still required, but no H₂ or CH₄ was used, and heat from the pyrolysis of the biomass was shown to partially offset the energy consumption. The authors also conducted a life-cycle assessment to demonstrate the reduced health, eco-system, and resource impacts of their synthetic method as compared to traditional methods.

Chemical exfoliation, the harsh oxidation of graphite followed by reduction, has seen an abundance of study to improve methods as well as to lower the waste chemical footprint. One such high profile example is from Pei et al. wherein two simple electrochemistry reactions in sulfuric acid can result in the oxidative exfoliation of graphite without the use of any other chemicals or oxidizing agents, in a process much faster than traditional Hummers' type oxidations.^[116] When compared to graphene oxide produced by traditional methods, very similar materials properties were achieved, and excitingly all the sulfuric acid was able to be recycled, minimizing the waste generated by this process, and even 90% less rinse water was used. The authors went on to demonstrate a continuous production prototype, and to discuss the mechanism for oxidation, while demonstrating applications of graphene oxide in aerogels, films, and carbon papers.

Sustainable reduction of graphene oxide has received much study as it is the unavoidable counterpart in chemical exfoliation following oxidation. The type of reducing agent has seen the most work, with groups using sustainable or solvent-free reducing methods. New sustainable chemical reducing agents, taking the place of harmful hydrazine or hydroiodic acid, have been reported ranging from plant extracts and lemon juice to ascorbic acid and green tea, however, these methods still generally consume large amounts of water or other solvent.^[63,117–119] Solvent-free methods of reduction greatly reduce economic/environmental footprints and process mass intensity, and a traditional method is to use thermal reduction in a furnace. However, recent examples have leveraged hydrogen plasma, microwave radiation, or even the use of Xe lamp radiation to reduce graphene oxide to graphene-like materials.^[120–123]

One advance to decrease the large process mass intensity required by physical exfoliation (1000 L of solvent per kg of graphite, typically) came from Dong et al.^[124] They demonstrated that pretreatment of graphite in sulfuric acid with a single equivalent of KMnO₄ (as compared to the large excess needed in Hummers' method) allowed for extremely easy exfoliation to graphene using shear mixing. Only a 3.6% increase in oxygen content was observed by XPS analysis, low defect concentrations were observed by Raman spectroscopy, and 1–2 nm thickness was seen by AFM. Most importantly, they reported that their process allowed for graphene slurries as concentrated as 50 mg mL⁻¹ in pH 14 solutions with yields as high as 82.5%. This allowed for significantly decreased amounts of solvent required for physical exfoliation. Further, production of 1 kg of graphene was reported, and rates as high as 80 g h⁻¹ were calculated. Other examples of efforts to increase the sustainability of physical exfoliation methods include the use of naturally

abundant surfactants and dispersants. One recent report used tannic acid, one of the most naturally abundant organic compounds, as a dispersing and surface stabilizing agent during sonication to achieve higher concentrations and yields per unit solvent used.^[125]

Several studies have demonstrated the use of biomass or waste materials as precursors to synthesize large amounts of graphene materials or graphite nanoplatelets. The waste materials often require extensive pretreatment, milling, or washing, before undergoing high-temperature pyrolysis under an inert atmosphere, followed by etching or activation. These products are also generally lower quality and demonstrate high defect concentrations, low overall crystallinities, and low levels of carbon purity. Despite this early work yielding low-quality products, it is encouraging to see the effort to leverage waste materials as precursors and upcycling them into high-value products with demonstrated applications. One such example is the conversion of waste biomass into a relatively high quality 1–5-layer graphene in a "solvent-free" method using dry shear mixing of biomass with simple iron salts followed by carbonization and graphitization under inert atmosphere at high temperatures.^[126] However, rinsing with HCl is still required to remove excess iron, so the classification of this method as solvent free is somewhat imprecise.

1.6. Prospects and Outlook of Academic Larger-Scale Graphene Production

Just as industrial graphene production can benefit from a standardization of terminology and characterization, many research articles on graphene synthetic methods are making graphene nanoplatelets with >10 layers. Greater care is needed in standardization. Similarly, average Raman spectra should always be shown, with Lorentzian fitting and reports of pertinent peak full-width at half maximum (FWHM). AFM is helpful for good quality graphene characterization since it is an excellent method to arrive at an average thickness of particles produced through synthesis. Average thickness, since it directly relates to the classification of the graphene material, is an important feature. Often, especially in manuscripts detailing top-down exfoliation methods to synthesize graphene, no yield or estimated production rate is given, and thus the scalability of the method is impossible to assess. A simple mass balance, graphite input vs graphite removed after centrifugation, and extrapolated graphene produced in solution, should be included. A UV–vis measurement extrapolated to yield of graphene synthesized can greatly ease the comparison of literature methods. These simple standards would result in easier comparison between methods and possibly faster translation to commercial scale-up or application.

The larger-scale graphene production methods presented in Section 1 (200 mg or 200 cm² films), both industrial and academic, have various considerations when scaling. Environmental and safety concerns, such as the use of high-purity inert or flammable gases, flammable solvents, explosive oxidizing/reducing agents, or strong acids can complicate the scale-up and industrialization of academic advancements. The handling of waste streams and byproducts, especially in chemical exfo-

liation methods, can pose a significant cost and complicate scale-up. Thus, efforts to avoid the use of expensive or hazardous reagents can improve the potential and ease of scale-up. For example, potassium permanganate in sulfuric acid, as commonly used for oxidative exfoliation pathways, is explosive when concentrated thereby exacerbating disposal.^[62] Use of alternative oxidation methods can result in competitive economic processes and they will ultimately result in a less expensive product if waste mitigation costs can be minimized.

Even with physical exfoliation methods such as sonication, ball-milling, shear mixing, or multiroll milling, considerations of increasing from a bench-top scale are often not addressed. It is well-documented that the scalability of sonication is nonlinear with respect to yield or power demand.^[127] In solvent-intensive physical exfoliation strategies, such as sonication or shear mixing, re-use of solvent and surfactant are essential if the method is to be industrialized. Demonstration of solvent or surfactant recovery and reuse can greatly improve the economic viability and decrease environmental and disposal impacts, increasing the attractiveness of a process for scale-up. Alternatively, in bottom-up syntheses, the reuse of the growth substrate or use of lower-cost substrates are important considerations. As discussed previously, a powder phase product as opposed to a solvent dispersion presents many advantages in both shipping and downstream product implementation. However, fine dry powders must be checked for their explosive properties upon impact, and they might warrant water-wetting for safe transport and storage. Thus, academic methods that demonstrate and characterize powdered graphene products could have advantages.

In general, for both bottom-up and top-down synthetic methods that demonstrate larger-scale and hope to be scaled up, consideration of all steps in the process is essential. For example, the fast growth of large-area graphene films is certainly noteworthy and exciting, but consideration of the growth substrate preparation and graphene film transfer for terminal applications is essential. Life cycle assessments or technoeconomic analyses can reveal these oversights since it prompts the researchers to examine all production steps and possible pitfalls.

2. Flash Joule Heating

2.1. Flash Joule Heating Background

FJH has been known in the literature for many decades but was more recently applied to the synthesis of graphene.^[127–129] Most notably, rapid Joule heating has been reported in the sintering of ceramics for more than a decade, where current is passed through a lightly conductive compacted powder, internally generating heat.^[130,131] This heat generation, more than 1000 K min^{−1}, results in sintering of the ceramic or glass much more rapidly and efficiently than through the use of a furnace.^[132] The rapid heating and cooling rates of FJH have also been leveraged to synthesize metallic glasses since the rapid cooling rate kinetically limits the crystallization that is able to occur in the alloy mixture.^[133] FJH, known commonly as field-assisted heating or sintering, traditionally was produced by passing

direct current through high-pressure molds. Commercial field-assisted sintering technologies exist and are available for academic and industrial research and use, capable of exceeding 300 tons of pressure and sintering ceramics up to 35 cm in diameter.^[134] Generally, temperatures stay below 1500 °C during these types of sintering and that is often far lower than furnace temperatures needed for traditional sintering methods for the same material.

Several computational models and mechanistic studies exist to predict and explain the products obtained from flash sintering. Fundamental work on nanomaterials such as nanoscale grain and platelet Cu, Ag, and zirconia synthesis has occurred in the past few years.^[129,135–137] This brief introduction to applications that take advantage of rapid Joule heating caused by strong electric fields highlights that this is a robust field. FJH has achieved high levels of technological readiness and scale-up, and the work we present in the remainder of this review leverages this methodology with some important modifications.

2.2. Flash Joule Heating for Graphene Synthesis

FJH was used in 2020 by Luong et al. to synthesize gram-scale quantities of graphene from a variety of feedstocks including carbon black, coal, petroleum coke, waste foods, and plastics.^[30] The decision to apply FJH to the synthesis of graphene drew inspiration from LIG, where extremely rapid and localized heating is used to convert carbonaceous feedstocks such as polymer films or paper into metastable graphene foam in a bottom-up method. LIG shows great promise in direct-writing circuits and flexible electronic applications but does easily not produce true bulk graphene that is widely used in many of the other applications of graphene such as composites, lubricants, or coatings. Further inspiration was drawn from the work of Hu's group, who used ultrafast Joule heating to weld carbon nanofibers together to afford thin films with graphitic bonds and high conductivities.^[138] They reported heating rates of 200 K min^{−1} and peak temperatures of 2500 K. Inspired by LIG and Hu's ultrafast Joule heating,^[138,139] a graduate student, Duy Luong, set out to reproduce the rapid heating and conversion of carbonaceous feedstock into graphene on a larger scale. The graphene powder produced through FJH was demonstrated on a gram scale, and shown to be turbostratically arranged. It was among the first reports of gram-quantity, bottom-up synthesis of turbostratic graphene that was highly characterized.

The FJH strategy operates on the highly efficient conversion of electric current directly into thermal energy when it passes through a resistor. However, the amount of current, hundreds of amperes supplied by banks of capacitors is an essential feature. Thus, the capacitance of the capacitors used is essential in this FJH process. Another key feature is that in FJH, the resistor is composed of the carbon-based starting material, which is thus heated to very high temperatures, resulting in the cleavage of bonds and reorganization to the thermodynamically favored sp²-hybridization of graphene sheets. Graphene is the most thermodynamically stable form of carbon. Because of the temporally short nature of the “flash” of electric current, these graphene sheets do not have the opportunity to stack into the more stable and ordered AB layering of graphite, trapping them

in a metastable state known as turbostratic graphene. Due to the bright flash of black-body radiation emitted during the FJH current discharge, the produced product is also termed “flash graphene” (FG). Further mechanistic discussions are provided in Section 2.6. In the initial publications on FJH of amorphous carbon to form grams of turbostratic graphene, amorphous carbon black as a starting material was studied extensively, though the method was shown to work on many other carbon feedstocks.

Using Raman spectroscopy, which will be discussed in more detail in Section 2.5, extremely high-quality graphene is demonstrated to be produced using this flash method, as exemplified by extremely low defect concentrations shown by the small D peak, and long-range crystallinity seen by the height and FWHM of the 2D peak. The duration of heating, as controlled by the duration of current discharge through the carbon sample, was also determined to directly impact the quality of graphene produced (Figure 5a). Overall, yields of graphene from amorphous carbon black ranging from 80–90% are achievable using FJH, and carbon purities more than 99% are regularly observed. Most excitingly, at no point is solvent or inert gas used during the synthesis of flash graphene, and scales larger than 1 g per batch were demonstrated. Production rates of ≈75 g h^{−1} were demonstrated at the time of the first publication. Bulk conversion into graphene using FJH can readily afford mass yields >90% based on the amount of carbon present in the precursor material. Large-area Raman spectral mapping demonstrates that often ≈100% of the product is graphene. Contaminants that may be present in starting materials, such as trace metals, silicon, aluminum, or other heteroatoms sublime out during the FJH process. Carbon has the highest sublimation point of all elements. In all FG manuscripts, no further purification is used for FG that is used in composite or energy-storage applications. Likewise, no further purification is used prior to the characterization of the FG. However, if extremely high-purity FG is desired, trace highly carbonized impurities can be removed through dispersion and centrifugation, or through calcining since the thermal stability of graphene is higher than that of amorphous carbonized impurities. Both methods are scalable and used industrially. These methods have not, to our knowledge, been demonstrated in FG systems but have been used in other graphene synthetic methods. Dispersion and centrifugation take advantage of the very high surface area of graphene sheets, which disperse better than aggregated amorphous carbon impurities. Centrifugation can then be used to remove the impurities or other aggregates. This strategy is commonly used in the field to prepare AFM samples and is like solution-phase exfoliation strategies. A comparison of FJH to other recent and promising larger-scale graphene synthetic methods is presented in Table 1.

Complete conversion to crystalline graphene can be observed through powder XRD (Figure 5b), which shows the intense (002) peak centered at 26.1°, corresponding to an interlayer spacing of 3.45 Å. This interlayer spacing is significantly larger than the 3.36 Å that is commonly reported for graphite. Further, the FWHM of the (002) peak is larger, and the peak is asymmetric toward low diffraction angles, suggesting that a wider array of stacking environments occurs when compared to graphite. The stacking of turbostratic graphene sheets produced by FJH can

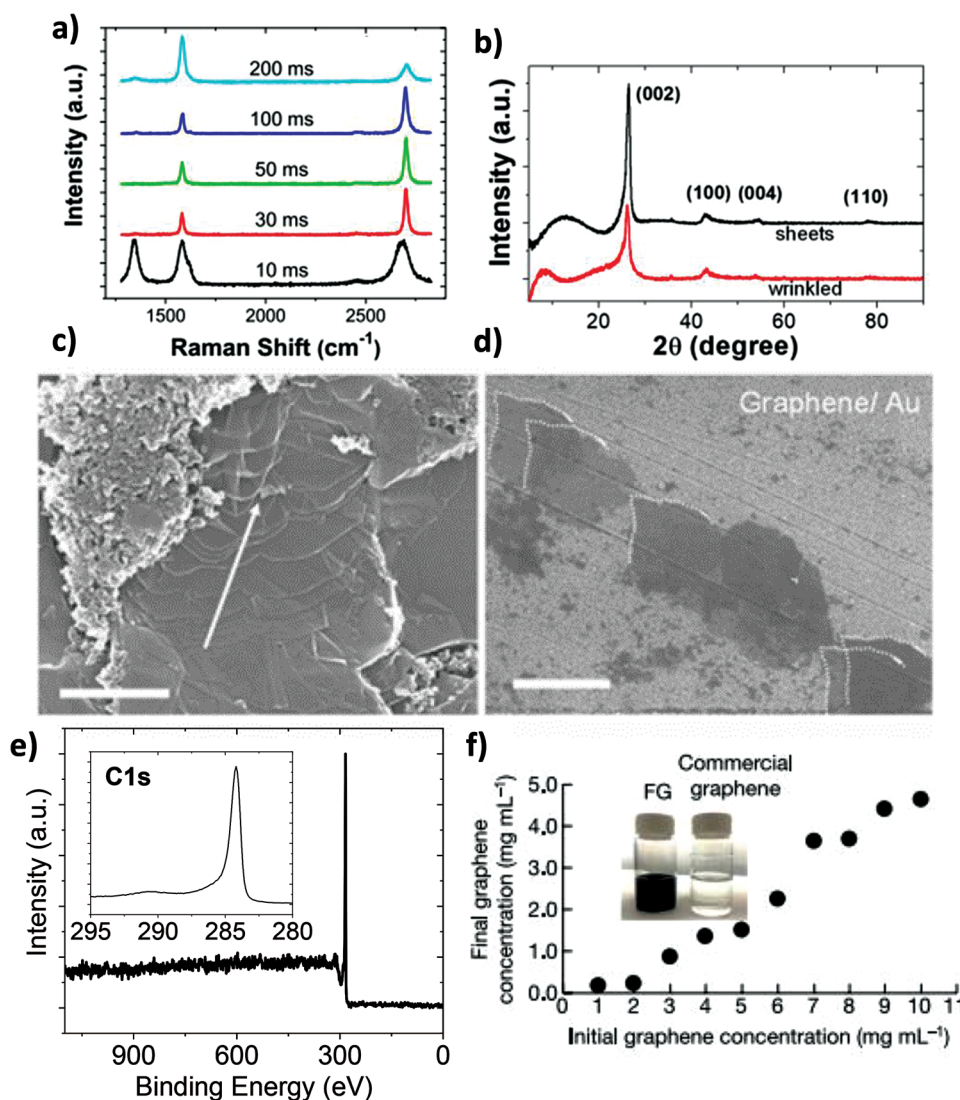


Figure 5. a) Raman spectra of flash graphene samples, as a function of FJH duration. b) Powder XRD spectra of two morphologies of flash graphene. c,d) SEM images showing a stack of flash graphene sheets, which are then exfoliated through simple shear force along the surface (scale bar is 500 nm). e) XPS analysis of flash graphene with inset high-resolution XPS of the C1s binding energy region. f) Dispersions of flash graphene in 1% surfactant aqueous solution, as compared to commercial graphene in the optical image. a–d) Reproduced with permission.^[33] Copyright 2020, American Chemical Society. f) Reproduced with permission.^[30] Copyright 2020, The Authors, published by Springer Nature.

be observed via SEM as shown in Figure 5c to form large crystal domains of these loosely interacting sheets, so decoupled that they can be easily exfoliated (Figure 5d). Elemental purity and a better understanding of the carbon bonding can be afforded by XPS analysis (Figure 5e). Elemental purities above 99% carbon content can be achieved when using amorphous carbon black as the feedstock, and 98.6% sp² hybridization can be observed using high-resolution XPS.

Due to the observed increase in interlayer spacing, it was hypothesized that the turbostratic graphene would allow for higher dispersibilities as it can easily be exfoliated to single layer thicknesses. The addition of flash graphene to a variety of organic solvents, as well as a 1% surfactant-assisted aqueous solution, yielded a high concentration of very stable dispersions (Figure 5f). These dispersions did not exhibit any settling out of

graphene aggregation, even when stored for many months, in contrast with the poor stability of the commercial graphene dispersions. Preliminary cost analysis was conducted in the initial publication as well, demonstrating that only 7.2 kJ of electricity are required per gram of graphene produced, and ≈\$100 of electricity costs per ton of graphene produced.

The current discharge through the resistive sample results in extremely high temperatures being produced, up to 3200 K in less than 10 ms (Figure 6a), indicating the formation of defect-free graphene sheets that are rotationally disordered (Figure 6b–f). This rotated orientation can be confirmed optically as well, through the use of TEM imaging to observe Moiré patterns present as well as the selected-area electron diffraction (SAED) pattern which shows two sets of distinct six-membered rings mismatched by 9.93°. This rotation allows for the

Table 1. Comparison of recent academic larger-scale graphene production methods, contrasting production rates and quality of products.

Method	Product	Estimated production rate	D/G ratio	2D/G ratio	Thickness (AFM)	Carbon content (XPS)	Refs.
Plasma exfoliation of graphite	1–3 layer graphene powder	48 g h ⁻¹	0.15	0.75	0.8 nm	95.50%	[98]
Electrochemical exfoliation of graphite	Vacuum-dried few-layer graphene	30 g h ⁻¹	0.14	0.36	4 nm	93%	[140]
Electrochemical exfoliation of graphite	Vacuum-dried few-layer graphene	25 g h ⁻¹	0.08	0.4	1.5 nm	96%	[95]
Detonation of acetylene in oxygen	Few-layer graphene powder	25 g h ⁻¹	0.2	0.75	–	98%	[112]
Arc discharge through graphite electrodes	Few-layer graphene powder	12 g h ⁻¹	0.51	1.03	1.9 nm	97%	[99]
FJH of carbon feedstock	Tubrostratic graphene powder	7.5 g h ⁻¹	0.08	1.1	1.2 nm	99%	[30]
Solvent assisted shear multi-roll milling	Dispersed graphene nanoplatelets	6 g h ⁻¹	0.1	0.71	15 nm (TEM)	–	[92]
Shear mixing of graphite in solvent	Dispersed few-layer graphene	5.3 g h ⁻¹	0.17	0.26	7.3 nm	>90%	[89]
Surfactant assisted milling of graphite	Dispersed few-layer graphene	2.5 g h ⁻¹	0.65	0.25	3.5 nm	–	[141]
Electrochemical exfoliation of graphite	Freeze-dried few-layer graphene	2 g h ⁻¹	0.45	0.94	–	96%	[97]
Bromine intercalation and microwave exfoliation	Few-layer graphene powder	1.5 g h ⁻¹	0.09	0.48	1.1 nm	95.3%	[94]
Supercritical CO ₂ assisted sonication	Dispersed few-layer graphene	0.5 g h ⁻¹	0.2	0.4	1.5 nm	–	[93]
Salt intercalation of graphite	Dispersed few-layer graphene	0.4 g h ⁻¹	0.1	0.45	2.6 nm	99%	[142]
Electrochemical intercalation followed by sonication	Dispersed few-layer graphene	0.3 g h ⁻¹	0.25	0.4	5.2 nm	–	[96]
Acid and peroxide assisted exfoliation	Dispersed few-layer graphene	0.25 g h ⁻¹	0.05	0.88	1 nm	97%	[143]

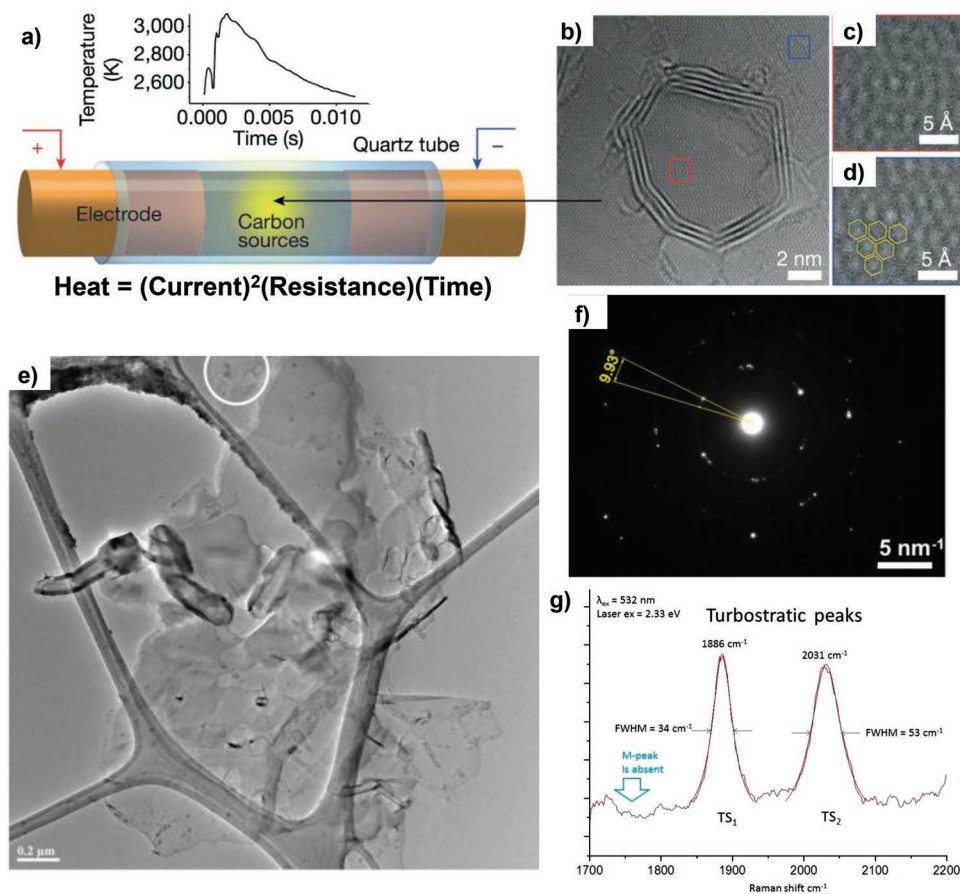


Figure 6. a) Schematic of the FJH process, and plot of temperature versus time during (inset). b–d) HAADF-STEM images of FG on top of a larger sheet of FG. e) HR-TEM images showing a large flake of few-layer graphene derived from coffee. f) SAED of the circled area in (e) demonstrating the misorientation of graphene layers and g) high-resolution Raman spectroscopy confirming the turbostratic stacking. a–g) Reproduced with permission.^[30] Copyright 2020, The Authors, published by Springer Nature.

lessening of van der Waals interactions, permitting facile dispersion as described. TEM analysis can further observe an increase in interlayer spacing in the lattice fringe of 3.45 Å, which is significantly larger than the 3.34 Å spacing observed in AB graphite. To further probe the discussed turbostratic arrangement of the bottom-up synthesized graphene sheets that allow for easy exfoliation and high concentration dispersions, high-resolution Raman spectroscopy and TEM imaging was carried out. Specific details and further discussion on the interpretation of Raman spectra of larger-scale graphene powders are provided in Section 2.5, but the presence of the TS₁ and TS₂ peaks, with locations and widths matching well with literature values, is strong evidence of the rotational disorder that is present in the sample (Figure 6g). The very high 2D/G ratios (with the 2D peak being up to 17 times more intense than the G peak) are further confirmation that the produced flash graphene is composed of multilayer turbostratic graphene.

In the initial publication, the authors also demonstrated multiple applications of the flash graphene, such as increasing the compressive and tensile strength in cement by up to 35% with just 0.1 wt% addition of FG.^[30] The enhancements in compressive strength were found to greatly outperform composites using electrochemically exfoliated graphite, even at the same mass loading. Poly(dimethylsiloxane) (PDMS) composites showed 250% increases in compressive strength as well, when 0.1 wt% flash graphene was added. Initial studies demonstrating the use of flash graphene derived from amorphous carbon black as an electrode material in Li-ion capacitors and batteries were also conducted, but optimization of capacity and stability is still required in these areas.

As with all research, the technique, and more importantly the FJH equipment, went through many iterations of design to advance from one generation to the next, over a span of multiple years. To date, several FJH stations have been used, as described in **Figure 7**. As discussed above, the most important aspects of an FJH apparatus are the capacitance of the capacitor banks, discharge control system for controlling heating, and system safety. Advancements in the sample holder and reaction chamber have also occurred through each iteration. These improvements allowed the batch size to move from 20 mg in FJH Beta up to 1.1 g in FJH V2 as the capacitance of the system increased from 10 to 200 mF. FJH Beta and V0 used simple toggle or disconnect switches, rated for 50 A or below, and they were manually operated. Switches that are manually operated are undesirable, due to poor control and limited reproducibility, as well as safety concerns. FJH V1 and V2 ameliorated this by switching to a 100 A mechanical relay, which was driven by a simple Arduino and LCD screen interface, controlling the discharge with an estimated reproducible temporal resolution of ≈50 ms. Computer control was realized in FJH V3, using a simple LabView interface interacting with an I/O board that drives an insulated gate bipolar transistor (IGBT) for switching. Use of the 600 A rated IGBT enabled kHz frequency switching, allowing for sub-millisecond temporal resolution in the switching.

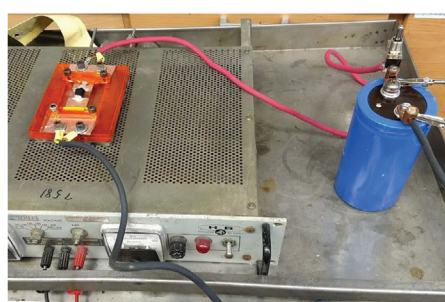
Major improvements in the analysis of the FJH process occurred through the construction of a spectrometer to record the temperature reached during the current discharge, determined through the fitting of the emitted black-body radiation.

The spectrometer was made in-house using a fiber optic cable to collect and transmit the radiation onto a grating followed by a photodiode array. The signal is then conveyed to a computer interface through an I/O device. This spectrometer was implemented beginning in FJH V1. To better understand the role of current discharge through the sample as it converts into flash graphene, a Hall effect sensor was installed on FJH V3. This allowed for the extremely high-resolution recording of the current discharge over time, which has enabled precise energy consumption calculations as well as a better understanding of how peak current or total current impacts the temperature and thus the quality of graphene produced. Since the assembly of FJH V3, multiple other designs have been constructed to incrementally improve the utility, scale, or function. FJH V4 is discussed later in this review, and newer versions will be disclosed in manuscripts currently under preparation.

Due to the in-house construction of the FJH instrumentation as well as the high voltages and currents used, we understand that entrance into the field of FJH might be difficult for some research groups. Hence, we provide here a brief discussion of the design and safety considerations determined from our five years of study. Primarily, the construction and operation of the FJH system, like much equipment or procedures in any research laboratory, can be hazardous, but the hazards can be minimized through proper experimental design, training, and use. Surely, electrocution is a hazard and steps must be taken to minimize that risk. Most importantly, proper training of all users is essential. Consultation of an electrical technician during the design and construction of an FJH is essential. It is important to use wires and components able to safely operate at high voltages and currents. There should be multiple visual in-line indicators of instrument charge and status such as light bulbs or LEDs. Multiple kill switches should be installed, preferably in the form of steady-state high direct current-rated circuit breakers since they inherently suppress arcs. As a rule of thumb, transformers, if used, and capacitors are the most dangerous aspects of this system, and if not properly designed, charge from these components can appear in unexpected places. Capacitors, if no resistor is present to slowly bleed off the charge, can indefinitely hold dangerous levels of charge, so the use of large 100 000 Ω bleed resistors is important. Thick insulating gloves extending to the elbows should be worn when the FJH is being used, and components should only be touched in a discharged and disconnected state, using one hand, and making sure the operator is not otherwise grounded. Bright flashes of black-body IR and visible photons are emitted, so the use of an opaque reaction chamber or dark glasses is suggested. Welding or brazing safety glasses provide protection from both UV and IR radiation, and a minimum shade number of #3 is recommended. Our several publications using the FJH station provide detailed electrical schematics and safety lists.^[30,31,33,34]

2.3. Flash Graphene from Waste Materials

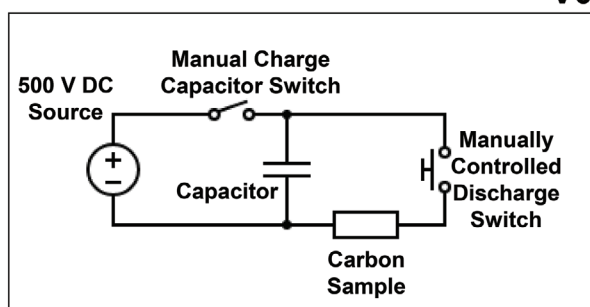
The conversion of amorphous carbon black into grams of turbostratic graphene was used for initial optimization, but the use of other high-carbon content feedstock materials, such as anthracitic coal, calcine coke, and charcoal demonstrated process



**FJH
Beta**



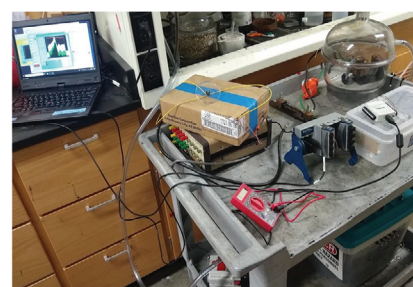
**FJH
V0**



**FJH
V1**



**FJH
V2**



**FJH
V3**

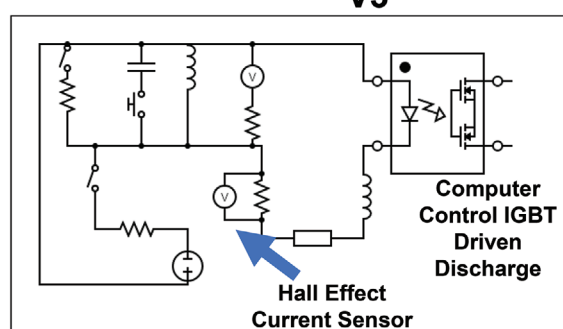
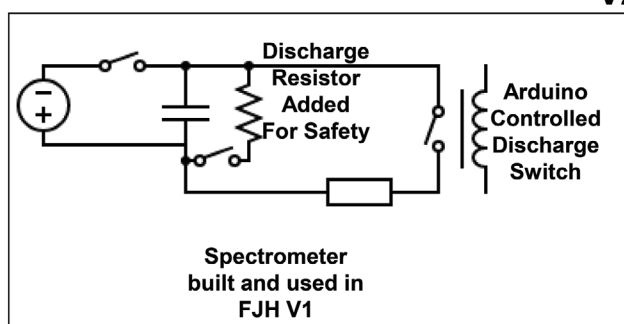


Figure 7. Photographs and simplified circuit schematics displaying the evolution of FJH stations. Each circuit schematic highlights the important advances in current discharge control and process analysis added with each iteration. The 500 V DC source is provided by a transformer, and varying amounts of capacitance were used in each version. The carbon-source sample holder is represented in all schematics by the square load resistor as labeled in the first circuit schematic.

generality. Several low-value and waste materials were studied as carbon feedstocks as well and were included in the original publication.^[30] Biochar, humic acid, keratin, lignin, sucrose, starch, pine bark, olive oil soot, coconut char, coconut shells, coffee grounds, pistachio shells, potato skins, waste rubber, and rubber-tire-derived carbon black were all able to be converted into graphene using the

FJH process. A variety of other waste carbon feedstocks have been screened at the request of collaborators and remain unpublished, yet we have not encountered a dry, high-carbon-content material that cannot be converted into graphene through FJH.

Through select optimization of the FJH parameters such as sample mass, resistance, voltage, and duration of discharge,

the quality and elemental purity of the produced graphene derived from pyrolysis ash and waste rubber was greatly improved. Hoping to further demonstrate and capitalize upon the ability of FJH to convert zero- or negative-value materials into high-value graphene, a more in-depth study was dedicated to ash resulting from the chemical recycling of waste plastic (pyrolysis ash) as well as waste rubber tires and rubber tire-derived carbon black.^[31,32] Pyrolysis ash and tire carbon black are unavoidable byproducts of the catalytic depolymerization of plastics and tires and are high in carbon content but contaminated with trace metals and other undesirable impurities. Hence, some optimization of pretreatment FJH pulses proved to be important when using larger weights and less pure feedstocks since this treatment aids in the precarbonization of the low-carbon-content materials. This can result in 90–95% graphene yields based on the initial carbon content with 50–80% overall weight yields depending on the feedstock. Further, 94–98% elemental carbon purity was determined by XPS. High average 2D/G ratios of ≈ 0.8 and excellent dispersibilities were observed. Plastic-derived pyrolysis ash produced some sheets that were hundreds of nanometers in lateral size, while tire carbon black and waste rubber produced smaller-sized sheets of 3–40 nm. Both feedstocks showed an increased interlayer spacing as compared to AB-stacked graphene, when analyzed by TEM. These waste material feedstock-derived flash graphene products were all tested in Portland cement and concrete, showing 25–43% increases in compressive strength at addition amounts < 1 wt%.

The plastic waste pyrolysis ash-derived turbostratic graphene was also dispersed in PVA to enhance the properties of the biodegradable polymer. Significant decreases in water uptake, absorbing 20% less water than the control over 10 d, and increases in hydrophobicity with contact angle of 56° compared to 24° in the control sample, were observed. Further, the produced graphene-enhanced PVA films showed up to 30% increases in toughness and failure strain. These negative-value waste and byproduct materials could be converted into valuable graphene and demonstrated multiple composite applications, in hopes of economically incentivizing the recovery and chemical upcycling of plastic and rubber waste.

2.4. Flash Graphene from Waste Plastics

One of the most notable carbonaceous waste materials is waste plastic since its pollution continues to be a global focal point. Recycling of waste plastic is troubled by low economic viability, but also by the mechanical and chemical intensity required. Sorting of mixed plastic waste is almost always necessary before the various polymer types can then be cleaned in a water-intensive process, and finally undergoing mechanical shredding and remolding or chemical depolymerization. These sorting and washing steps are the most unattractive industrially, and as advanced packaging containing multiple layers of different types of plastic become more widespread, the very mechanism of these recycling methods is threatened. Thus, advanced chemical recycling methods able to convert mixed waste plastics into high-value products are essential.

Plastics inherently are insulating. For FJH, some level of conductivity is essential, thus the addition of 10 wt% carbon black or flash graphene from a previous run was required to make the mixtures conductive. This addition of a conductive additive, coupled with pretreatment discharges afforded graphene synthesis from many different types of plastics as well as mixed waste plastics, as disclosed in the initial publication.^[30]

Further effort to reduce the amount of conductive additive was studied, which resulted in the use of a two-step method.^[34] Through addition of small amounts (2–5 wt%) of conductive additive, such as amorphous carbon black or flash graphene, to fine ground waste plastics (**Figure 8a**), the resistance decreased to 100 Ω for 500 mg of plastic packed into a 8 mm diameter quartz tube. This resistance was then suitably conductive to pass current through, first using a long discharge of the capacitance banks. The current would initially remain very small, but as heat is generated through the Joule heating, the plastic will eventually begin to carbonize, and the resistance will decrease, allowing more current and thus more heat to be generated. To further simplify the technique and remove the need to use capacitors for carbonization, a new FJH system (FJH V4) was constructed, consisting of a 120V/60A outlet, and two 10 A circuit breakers, with the constant voltage provided by the laboratory electrical outlet, and the circuit breakers controlling the peak current delivered to the plastic. Due to the use of unrectified AC, this low-current FJH is also termed AC-FJH. The circuit breakers thus trip once the current exceeds 10 A, signifying that a resistance of $< 12 \Omega$ had been reached within the carbonized plastics. During this low current yet long duration carbonization step (0–10 A, over 8 s), temperatures > 2900 K are reached, as determined by the black-body radiation emitted during the process. At this point, the plastic is converted into carbonized low-quality graphene. It can further be converted into higher-quality graphene through a secondary traditional FJH discharge as described in Section 2.2, and it was shown that any plastic stream including mixed or unwashed waste plastic can be used without impacting the quality of turbostratic graphene produced. Raman spectra of the graphene following low-current AC-FJH carbonization and after the final high current FJH are shown in **Figure 8b,c**.

This FJH resulting in carbonization of the mixed waste plastic allows for direct conversion of waste plastic into graphene, without any intermediate pyrolysis processing. Further, since the heat necessary is generated in situ, there is no need for furnaces or inefficient heat transfer. The authors also observed that hydrocarbons such as waxes, oils and oligomers were emitted during the low-current FJH process, much like they are during the chemical recycling of polymers. Applications of the flash graphene powder were demonstrated, including the dispersion of the flash graphene in an aqueous-surfactant solution, resulting in 80x higher stable dispersibility than commercial thermally expanded graphite. The addition of the mixed-waste-plastic derived turbostratic flash graphene once again resulted in a 30% increase in compressive strength when 0.035 wt% is added to Portland cement. A preliminary cost analysis was also carried out, arriving at an estimated cost of \$124 in electricity to convert 1 ton of mixed waste plastic into 180 kg of turbostratic flash graphene.

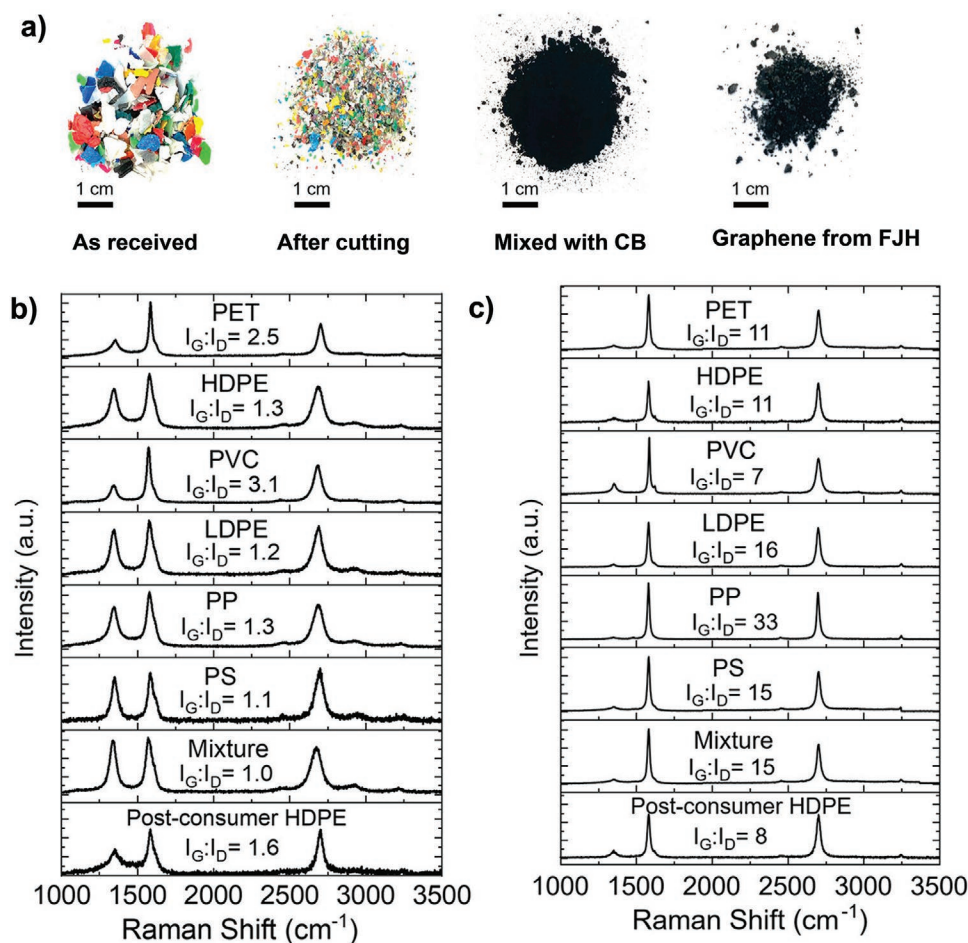


Figure 8. a) Photographs showing the process workflow to convert postconsumer high-density polyethylene (HDPE) into graphene (the conductive additive, carbon black is abbreviated CB). b) Raman spectra of graphene resulting from the AC-FJH carbonization of various types of plastic (poly(ethylene terephthalate) is abbreviated PET, poly(vinyl chloride) is abbreviated PVC, low-density polyurethane is abbreviated LDPE, polypropylene is abbreviated PP, and the plastic mixture is composed of 40% HDPE, 20% PP, 20% PET, 10% LDPE, 8% PS, and 2% PVC). c) Raman spectra of high-quality turbostratic FG produced after AC-FJH and high current FJH. a–c) Reproduced with permission.^[34] Copyright 2020, American Chemical Society.

2.5. Raman Spectroscopy of Graphene Powders

The use of Raman spectroscopy to characterize graphene and other 2D or nanomaterials is well described in the literature and multiple reviews.^[144–146] Raman spectroscopy is widely used, and generally accepted as the gold standard of graphene characterization, due to the vast array of information a single spectrum can provide. This includes the quality and symmetry of the graphene, as well as the stacking or translational organization of the neighboring sheets.^[147]

As discussed in Section 1.1, a rotational disorder of graphene sheet stacking allows sheets to maintain the optical and electronic graphene properties. This misorientation between graphene layers can be readily probed using Raman spectroscopy. The D, G, and 2D (also known as the G') peaks are readily present in turbostratic graphene; however, the intensity ratios may vary widely, especially throughout the entire sample. The common practice of assessing graphene layering through the 2D/G peak intensity ratio or FWHM does not apply to turbostratic systems. The individual layers are weakly coupled so the spectra remain independent of the number of layers. The

2D peak remains narrow and Lorentzian in shape; no additional modes are introduced at the K-point of the Dirac cone since no out-of-plane interactions are present.^[148] Due to this lack of intersheet interaction, the 2D peak remains a single peak that benefits from double-resonance enhancement, able to greatly enhance the peak intensity. In a reverse of AB-stacked graphite, where the 2D peak intensity decreases and loses the single Lorentzian shape as a function of number of layers, in turbostratic graphene the 2D peak retains its Lorentzian shape and can increase in intensity as more layers are present. 2D/G ratios as high as 17 can be observed in flash graphene turbostratic systems,^[30] while ratios higher than 2 are regularly be observed.^[149] This goes against the common notion dominant in CVD-grown graphene that the highest achievable 2D/G ratio is 4, occurring when a single layer is present. Further, the FWHM of the 2D peak in extremely high-quality turbostratic graphene can be as small as 15 cm^{-1} , which is smaller than the FWHM of documented single-layer CVD-grown graphene.

Other weaker and less-known peaks, namely the TS_1 , TS_2 , and M peaks are essential to understand the rotational alignment of graphene in powder form (Figure 6g).^[150–152] The TS_1

and TS_2 peaks are noted to occur due to combinations of transverse acoustic with the longitudinal optic or acoustic modes. The TS_1 and TS_2 peaks occurring at 1880 and 2030 cm^{-1} , respectively, when using a 532 nm excitation source, are generally ≈ 30 times less intense than the G band. The TS_1 can be fitted with a single Lorentzian and has a FWHM of $\approx 35 \text{ cm}^{-1}$, while the TS_2 is composed of two superimposed Lorentzians, thus having a slightly wider FWHM of $\approx 52 \text{ cm}^{-1}$. The M peak, which occurs at 1750 cm^{-1} when a 532 nm excitation source is used, is also a weak peak, $\approx 25\times$ less intense than the G peak, occurring well past the shoulder of the G peak. The M peak results from the combination of multiple phonon modes but arises from intersheet coupling and is thus indicative of AB stacking of multiple sheets. The M peak is notably silent when observing turbostratic graphene since these interlayer interactions are disrupted. When discussing graphene powder, or any turbostratic graphene products, all three peaks should be studied, with the presence of the TS_1 and TS_2 being apparent along with the absence of the M peak indicating a rotationally disordered product.

Larger-scale graphene production, whether top-down or bottom-up, will likely produce a distribution of graphene quality. Showing a single Raman spectrum for a production method can be misleading. Displaying an average spectrum, where each spectrum is normalized, then summed with many other spectra, from a wide area of a sample area, called a Raman spectral map over a large area, is therefore helpful. Or, producing scatterplots displaying the intensity ratios of important peaks from many spectra can be an aid in assessing larger-scale graphene quality. Raman spectrometer software often makes these plots accessible, and there are libraries of R or MatLab open-source packages that also do this. Therefore, Raman spectroscopy can be used to improve the comparison and reproducibility of larger-scale graphene production methods.

Preparation of flash graphene samples with varying ratios of ^{13}C and ^{12}C has permitted the further study of the optical and electronic properties using Raman spectroscopy.^[35] Due to changes in the lattice symmetry and vibrational frequencies experienced by the graphene sheets, unusual enhancements in the D' peak are observed. This indicated a favoring of intravalley phonon scattering modes in graphene lattices with 5–15% added ^{13}C . Also, Raman spectroscopy demonstrated high degrees of isotopic homogeneity, as a single set of D, G, and 2D peaks with minimal broadening were observed rather than doublets where one set pertains to graphene sheets of separate isotopic content. Interestingly, infrared analysis of a 1:1 ^{12}C : ^{13}C flash-graphene sample showed the long-sought carbon–carbon double-bond stretch at 1562 cm^{-1} due to the disruption of lattice mass symmetry.

2.6. Mechanism for FJH Graphene Synthesis

Mechanistic understanding is central to the optimization and advancement of graphene synthetic methods. In top-down preparation of graphene, the graphene sheets are already fully formed and the interest centers around the mechanism of exfoliation.^[153] Significant research interest also remains pertaining to bottom-up synthesis methods, searching for new catalysts,

lower temperatures, and more rapid formation of CVD graphene synthesis.^[154]

A current study shows that the FJH mechanism of graphene formation has most in common with thermal annealing and graphitization that takes place to convert amorphous carbon into graphite, which has been known for more than a century in the production of highly oriented pyrolytic graphite.^[155] This conversion from amorphous carbon begins at $>1000^\circ\text{C}$ as structural changes begin to take place, with the rearrangement and re-hybridization occurring as the activation energy needs are met.^[156] Rosalind Franklin conducted a study more than 70 years ago varying the carbon graphitization temperatures and observed the crystalline growth of graphite.^[157] She studied various amorphous carbons heated between 1700 and 3000 $^\circ\text{C}$, and measured the amounts of crystalline graphite produced using XRD. Two distinct classes of materials were found, graphitizing carbons which readily form dense graphite, and nongraphitizing carbons which formed a less ordered and more porous graphite structure. In the years since Franklin, researchers have studied graphitization in real-time using electron microscopy and they observed the formation of many carbon structures besides graphitic sheets.^[158] Many researchers have used density functional theory (DFT) or molecular dynamics (MD) simulations to study the structure of amorphous carbon materials and how they change during high temperature treatment, largely surrounding the annealing of carbon fibers.^[159]

For FJH synthesis, large-scale simulations have been used to further elucidate this graphitization and annealing process that happens on the millisecond time frame. Using these simulations, the density of carbon packing and temperature were demonstrated to have large impacts on the annealing process and most significantly on the final sp^2/sp^3 ratio obtained after annealing. The computational data, particularly demonstrating the temperature correlation with graphene formation and defect healing, agreed well with experimental results where the same phenomena are observed through Raman spectroscopy and TEM imaging. Due to computational constraints, simulations were constrained to less than 5 ns annealing at the given temperatures, and the resulting structures are shown in Figure 9a–c, with the change in hybridization shown in Figure 9d. Experimentally, temperatures during FJH are $>3000 \text{ K}$ for $\approx 5 \text{ ms}$, explaining how high-quality graphene can be obtained through rapid thermal treatment. Simulations have not been carried out to confirm that the turbostratic arrangement of graphene layers results from kinetic trapping due to the rapid cooling rate not allowing for ordered stacking of the layers into graphite. However, experimental studies have shown that extending the FJH times to 0.5 s results in a notable increase in AB stacking of the layers.^[33] SEM images suggest that along a single 1 mm-size crystal of turbostratic graphene, likely experiencing a large thermal gradient during synthesis, small-faceted graphene domains are observed. These "seeds" gradually merge and converge into larger graphene crystal domains. Raman spectroscopy demonstrates that at longer FJH pulse durations, AB stacking can be observed, lending credence to the mechanistic hypothesis that the rapid heating and cooling are essential to kinetically trap the metastable turbostratic product. Atomistic simulations were again conducted in this study, but probed longer durations up to 125 ns at maintained temperatures of

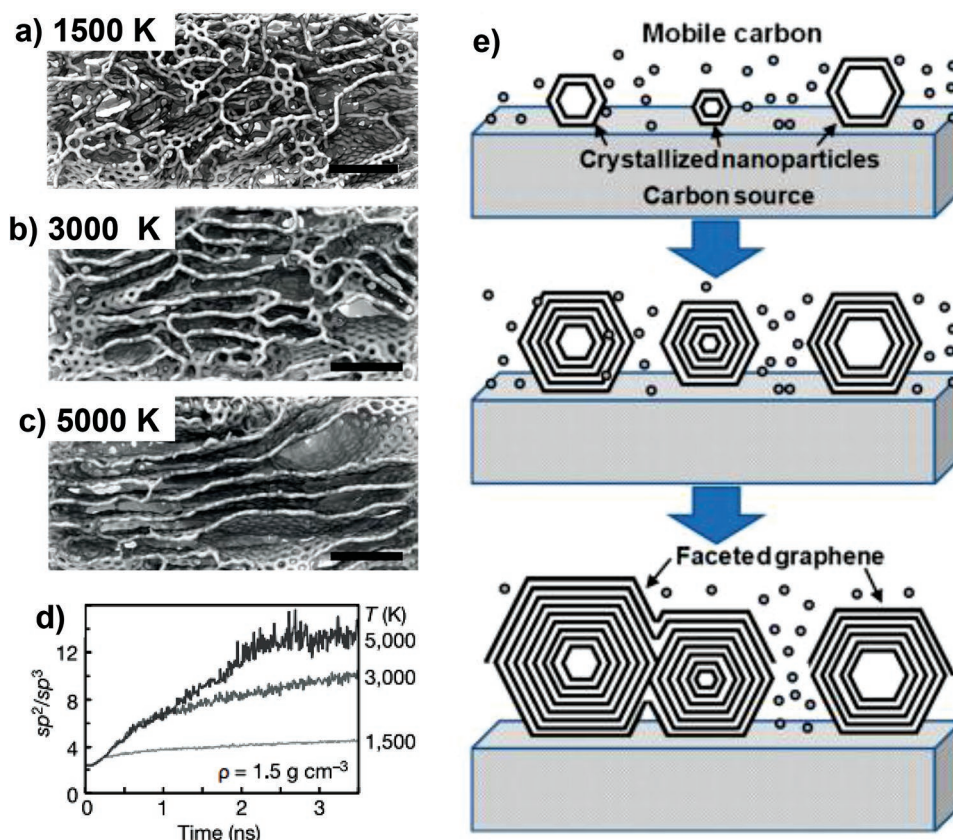


Figure 9. a–c) Molecular dynamics simulations showing the structure of materials with density 1.5 g cm^{-3} kept at different annealing temperatures for up to $5 \times 10^{-9} \text{ s}$ with a Nosé–Hoover thermostat. The scale bar for each structure is 1.5 nm. d) A schematic showing the proposed mechanism for graphene formation during FJH of carbon sources. b–d) Reproduced with permission.^[30] Copyright 2020, The Authors, published by Springer Nature. e) Reproduced with permission.^[33] Copyright 2020, American Chemical Society.

3500 K. Once more, extremely large increases in the sp^2 hybridization are observed, but molecular models still did not show distinct turbostratic graphene sheets being formed. The simulated time scale is only 0.002% of the duration that the amorphous carbon powder experiences during FJH annealing, but lack of sheet formation in simulations may indicate that factors such as electronic current or local fluctuation in charge or resistance, which are not accounted for in the MD simulations, may have sizable impacts on the FJH mechanism. Rather, MD resulting models show a wrinkled graphene structure, which is also observed experimentally and still shows turbostratic characteristics through expanded interlayer spacing by powder XRD. This wrinkled graphene morphology accounts for $\approx 60\%$ of the product and is still of high sp^2 content and elemental purity, while distinct sheet-like morphologies are observed for the remainder of the sample. These sheet and wrinkled morphologies are distinct optically as well as spectroscopically and may result from temperature or cooling rate differences during the FJH process.^[33]

Taken together, experimental and computational data present a mechanism for turbostratic flash graphene that involves the rapid heating due to electronic resistance, resulting in the rapid high-temperature annealing of the carbonaceous starting material. Carbon content increases during heating, since volatilization of noncarbon elements causes them to sublime or outgas

from the sample. During this annealing, mobile carbon is generated and begins to nucleate into thermodynamically favored sp^2 hybridized, faceted nanosized, or wrinkled graphene morphologies. These graphene seeds merge as heating durations are extended to 100–200 ms, giving rise to large domains of randomly oriented turbostratic graphene sheets, with increased interlayer spacing. Due to the high cooling rates, the orientation of the sheets to overlap the electron rich and poor regions of alternating sheets is limited since the thermal energy dissipates rapidly, kinetically trapping the metastable turbostratic product.

3. Perspective on Larger-Scale Graphene Synthesis

Helpful considerations for industrial or academic synthesis and use of larger-scale graphene include:

1. Stricter industrial quality control and certification of industrial graphene products are suggested. The overall poor quality of graphene on the market today delays successful application and depreciates the field of graphene research. Standardized characterization of graphene, such as presenting average Raman spectra, elemental purity information, standardized dispersibility data, and AFM or TEM derived sheet size and

- thickness, will increase the quality and utility of the "black powder" on the market today.
- Efforts to expand the use of green chemical methods are advantageous. The use of large amounts of solvent or water that is not easily recovered can lessen the attractiveness. The hope to recycle or upcycle waste materials, minimize waste streams, and minimize process mass intensity or process energy have all been demonstrated academically. Translation of these methods to industry should be investigated and implemented where possible. A wider utilization of strenuous life cycle assessments to better understand the impacts of graphene synthesis and applications can be used to identify problems and mitigate waste.
 - A better understanding of the environmental and biological impact of larger-scale graphene is needed. Fortunately, graphene is naturally occurring as crystalline aggregates of graphite and is present in coal in large amounts. Graphene may even shear from graphite in flowing river water. Further dedicated study on the retention and degradation of larger-scale graphene should be carried out at academic and industrial levels as graphene application increases.
 - Research collaborations between graphene manufacturers and commercial product users should be sought. Communication of desired characteristics and end goals can help tailor graphene products, resulting in the higher-quality implementation of graphene. Cross-industry or academic-industrial collaborations can also foster new graphene family materials applications, rather than following a one-size-fits-all use.
 - Sustained grant and commercial funding focused specifically on larger-scale graphene targets and applications should remain. Funding for improved graphene production research will in turn spawn further research due to increased accessibility of the materials needed.

To conclude our review of the larger-scale synthesis of graphene, the journey from Scotch-tape exfoliation to hypothesized production of kilograms or tons per hour, has not been linear or straightforward. Physical exfoliation and CVD growth of bulk graphene and graphene films, respectively, have dominated as the large-scale and industrial methods of choice. Few, if any, viable alternatives yet exist for the synthesis of graphene films outside of CVD growth, with many of the recent advances pertaining to the specific growth conditions and rates. These incremental advances are significant, but many challenges in cost, throughput, and final application remain to be addressed for the use of single-layer graphene films to fulfill the many desired applications. For the synthesis of bulk graphene, FJH represents just one exciting method to achieve high production rates. Top-down methods are limited by both the quality of starting graphite as well as the strong inter-sheet interactions, highlighting the utility of larger-scale synthesis of graphene using bottom-up methods.

4. Extensions and Outlook of Flash Joule Heating

4.1. Flash Joule Heating for Broader Materials Synthesis

As discussed, FJH is a powerful method to synthesize gram-scale turbostratic graphene from seemingly any high carbon-

content feedstock. However, FJH is not limited to graphene synthesis as recent publications have shown. In an extension of the synthesis of flash graphene, it was observed that while FJH fluorinated substrates, alternative phases of carbon could be synthesized.^[37] This work was further inspired by the small energy gap between formation of diamond and graphene, of 0.01–0.04 eV atom⁻¹ during synthesis.^[160] The phase transition of carbon through radical or transient intermediates also has been shown to have profound impacts on the final allotrope of the carbon product,^[161] and further work has shown that fluorination of the substrate can result in increases in radical stability during phase transformations.^[162,163] Thus, FJH of fluorinated organic carbon precursors was probed and resulted in controllable phase evolution. Fluorinated substrates included the use of Teflon and other perfluoroalkyl species. As previously discussed, low-current FJH results in carbonization to yield fluorinated amorphous carbon, which can then be further converted into fluorinated nanodiamond or fluorinated graphene products, before finally coalescing to form onion-like concentric carbon moieties (Figure 10a–c). High-resolution TEM, Raman spectroscopy, and XPS allowed for the characterization of the phase evolution. Microscopy shown in Figure 10 with accompanying FFTs demonstrate the shift from fluorinated nanodiamond (FND) to fluorinated flash graphene (FFG) and finally fluorinated concentric carbon (FCC) as the duration and peak current of FJH are adjusted. Raman spectroscopy in Figure 10d confirms the identity of each phase as well as demonstrates the turbostratic character of the FFG, since 2D enhancement is present. XPS analysis verified the presence of fluorine within the materials, showing fluorine content of 20% in FND, and lower contents of 3–7% in FFG and FCC materials. The C KLL, the measured energy of electrons ejected due to the filling of the K shell by an electron from the L shell coupled with the ejection of an electron from an L shell, was also probed using high-resolution XPS. This demonstrated predominantly sp³ hybridization in the FND samples and predominantly sp² hybridization present in the FFG and FCC materials.

This study is interesting not only because of the synthesis of other phases of carbon nanomaterials using FJH but because it sheds light on the process and mechanism of FJH, demonstrating how energy input influences phase transformation. Nanodiamonds had not been previously observed during the FJH conversion of amorphous carbon into graphene since the necessary electronegative fluorine was not present, and thus did not favor the formation of sp³ hybridized nanodiamond structure. Observed fluorine concentrations are lower in FFG and FCC materials which are only formed when higher energy densities are used, thus giving the system enough energy to form thermodynamically favored HF by breaking the C–F bond while forming the sp² hybridization. It is hypothesized, and observed via TEM imaging, that formation of the polyhedral FCC result from the surface graphitization of FND particles. Total phase purity was not attained during this study, and work continues to afford higher degrees of phase selectivity. Hence, the facile FJH synthesis of metastable phases, which are often more difficult to access was demonstrated.

Interestingly, FJH has recently been applied to the larger-scale synthesis of other 2D materials. The phase transformation of metastable 1T phase of MoS₂ and WS₂ was achieved thereby

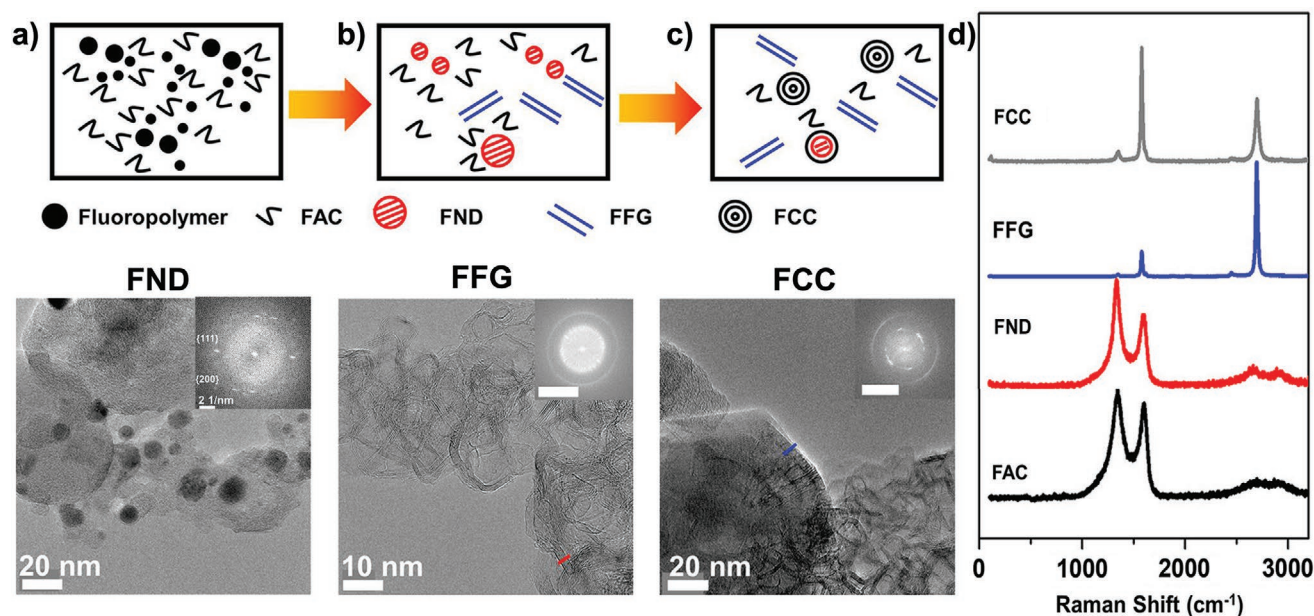


Figure 10. a–c) scheme showing the conversion of the fluorinated precursor to form FAC (a), FND (b), and FFG with FCC (c). d) Raman spectra of each phase observed during FJH. a–d) Reproduced with permission.^[37] Copyright 2021, American Chemical Society.

suggesting that FJH is a general approach to new materials classes.^[36] Transition metal dichalcogenides are an emerging 2D material that is being extensively studied. MoS₂ is just over 6 Å thick.^[164] These materials stack similarly to graphite, but in contrast they have a bandgap making them useful in transistors, spintronics, solar cells, photocatalysts, and electrocatalysts.^[165] Also, distinct from graphene, there are two metastable materials phases that exist in these transition metal dichalcogenides, that are distinguishable based on the coordination and space group, which can greatly affect their physical and chemical properties.^[166] In MoS₂, WS₂, and closely related materials, these phases are termed the 1T and 2H phases, and differ significantly in conductivity and application. The 1T phase is difficult to form and has low stabilities, making study difficult since large amounts of S–Mo or S–W bonds must break and simultaneously reorganize.^[167]

Once again, direct FJH was leveraged to introduce high energy densities extremely rapidly, followed by rapid cooling rates of $\approx 10^4$ K s^{−1} allowing conversion and access to the metastable 1T form. The dichalcogenide was used directly, only needing a 5% conductive additive of carbon black to lower the resistance enough for FJH. The reaction was run on hundreds of mg scales, reaching currents over 1000 A. The 1T product was characterized through changes in the Raman spectra, XRD, and characteristic binding energies, as well as atomic-level visualization through high-angle annular dark-field scanning transmission electron microscopy (HAADF-STEM). Ratios of up to 50% 1T were observed; the change in phase results in distinct changes in vibrational and bonding modes (Figure 11a), and conversion of 2H to 1T can be followed as the duration of the FJH is extended. Inspired by literature where electronegativity was observed to ease the phase transition, tungsten powder was substituted for carbon black as the conductive additive and afforded up to 76% conversion of 2H into the 1T form as determined

by high-resolution XPS (Figure 11b–d). HAADF-STEM images show the clear conversion of 2H into 1T as well (Figure 11e,f).

First-principles DFT calculations were conducted to probe the mechanism of conversion from the stable and energetically favored 2H structure to the metastable 1T phase. These calculations coupled with experimental validation determined that the FJH process induces defects through the rapid heating and possible sublimation of sulfur-inducing vacancies. These vacancies, coupled with the accumulation of negative charge that occurs during FJH, were calculated to drastically lower the energy required for conversion to the 1T phase. Application of the FJH produced majority-1T phase was shown by significantly improving both overpotentials (−491 to −221 mV) and Tafel slope (136 to 65 mV dec^{−1}) in the hydrogen evolution reaction. The 1T has more metallic electronic properties. Further, the layer number was observed to decrease, and the interlayer spacing increase, suggesting that the FJH transformed MoS₂ may be more dispersible and useful to cast films or in the formation of composites.

These two recent publications show that FJH undoubtedly has many applications in 2D, metastable, or nanomaterials synthesis and phase transformation. The demonstrated scalability of this technique was shown when synthesizing larger-scale graphene, and it will unlock new applications or research avenues when applied to these other materials that are able to be synthesized using FJH. Further work in the larger-scale syntheses of these and other targets continues. This technique could advance many other synthetic, separations, or phase-transformation-based research areas.

4.2. Perspective and Future Outlook of Flash Joule Heating

FJH, when applied to the synthesis of graphene and other 2D nanomaterials, was only disclosed in 2018. Hence questions,

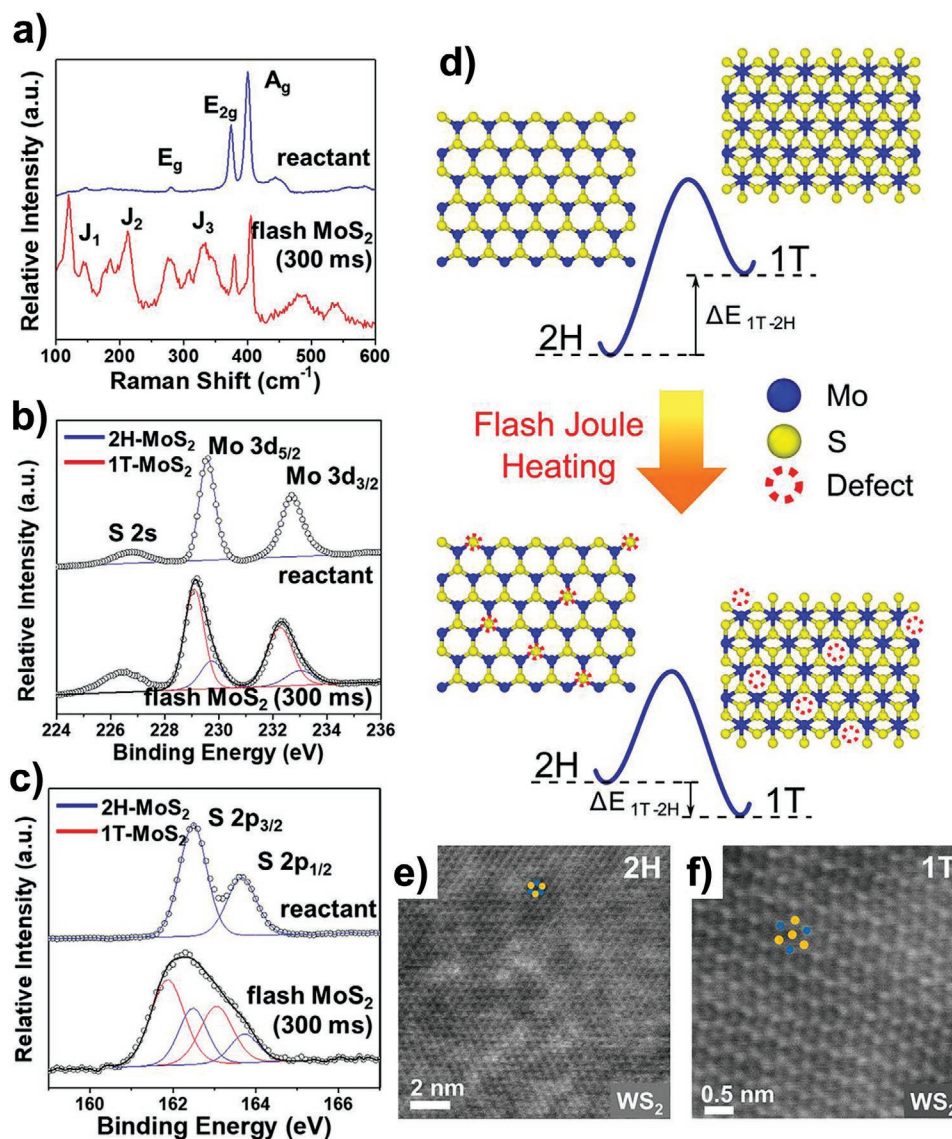


Figure 11. a) Raman spectra comparing the precursor 2H phase with the 76%/24% composition of 1T/2H phases that results from FJH. b,c) High-resolution XPS scans comparing the precursor 2H phase with the 70/30 mix of 1T/2H phases that results from FJH. d) A scheme demonstrating the FJH-assisted phase transformation of the 2H phase into the 1T phase. e,f) HAADF-STEM atomic images comparing the 2H and 1T phases (orange = S, blue = Mo). a–f) Reproduced with permission.^[36] Copyright 2021, American Chemical Society.

opportunities, and challenges remain. The further scale-up and commercialization of FJH for bulk synthesis of high-quality turbostratic graphene are currently being carried out by Universal Matter Inc. The company is scheduled to have a prototype manufacturing line operational in early 2022 and will represent the first industrial-scale, bottom-up graphene powder synthesis method. On an academic level, much work remains to be done to better understand and utilize FJH. Mechanistic studies, including simulations that account for the current and voltage contributions rather than simple heat annealing, will prove enlightening and will drive process optimization. Further experimental study of intermediate products and released volatiles, or in situ evaluation of intermediates and phase evolutions would greatly increase the mechanistic understanding of the FJH process.

The capability to convert a wide array of waste materials into high-value graphene through a generalized, facile process is also exciting and offers a host of potential applications. As discussed in Section 1.5, the trend of upcycling waste materials into graphene is not exclusive to FJH. These processes, and applications of the upcycled waste material-derived graphene, offer avenues to realize economic viability for responsible waste management and resource recovery. Use of other waste products in FJH, use of FJH to upcycle other high-value products, and use of FJH to lessen or eliminate of hazardous waste streams, are all possible future research directions.

One of the current shortcomings with FJH synthesis is the onerous trial-and-error optimization that is required when a new feedstock or reaction is being studied. The many reaction parameters that can be adjusted such as energy density and

heating rates are an advantage for specific materials design control, however, they result in significant amounts of time and characterization being required to incrementally synthesize and improve the desired product. Machine learning or simulation-guided optimization would be a powerful advance in this realm, and an area that is gaining precedent in materials synthesis.

Since FJH can afford other 2D, metastable, and nanomaterials, a new class of compounds will be accessible. Further, existing materials classes or phases may benefit from increased efficiency, scalability, sustainability, or feedstock generality. Likewise, new classes of materials, alloys, composites, or catalysts might be synthesized using FJH. FJH might be used as a simple rapid heating method to kinetically trap volatile products of interest and study their evolution based on peak temperature or reaction duration. From a more fundamental standpoint, the generation of heat in situ for a reaction, and ability to reach extremely high temperatures with rapid heating and cooling rates, could increase efficiency and decrease heat loss in several materials fields such as metallurgy. In conclusion, FJH for 2D materials synthesis is quite new. Yet its impact is being felt widely with respect to the attention received. This could be a harbinger for this classical method to be applied to new materials synthesis.

Acknowledgements

K.M.W. acknowledges the NSF Graduate Research Fellowship Program for generous funding. The authors thank the Air Force Office of Scientific Research (FA9550-19-1-0296) and the Department of Energy (DE-FE0031794) for their gracious support of FJH and other 2D materials research.

Conflict of Interest

Universal Matter Inc. and LIGC Applications Ltd. have licensed FJH and LIG approaches to graphene, respectively, from Rice University. J.M.T. is a stockholder in these companies, but not an employee, officer, or director. Potential conflicts of interest are mitigated through regular disclosures to and compliance with Rice University Office of Sponsored Programs and Research Compliance.

Keywords

2D materials, flash Joule heating, graphene, graphene industry, nanomaterials

Received: September 2, 2021

Revised: October 12, 2021

Published online: January 12, 2022

- [1] K. S. Novoselov, A. K. Geim, S. V. Morozov, D. Jiang, Y. Zhang, S. V. Dubonos, I. V. Grigorieva, A. A. Firsov, *Science* **2004**, 306, 666.
- [2] E. P. Randviir, D. A. C. Brownson, C. E. Banks, *Mater. Today* **2014**, 17, 426.
- [3] R. M. Desrosiers, D. W. Greve, A. J. Gellman, *Surf. Sci.* **1997**, 382, 35.
- [4] C. Oshima, A. Nagashima, *J. Phys.: Condens. Matter* **1997**, 9, 1.
- [5] A. M. Shikin, D. Farías, K. H. Rieder, *EPL* **1998**, 44, 44.

- [6] H. P. Boehm, A. Clauss, G. Fischer, U. Hofmann, in *Proc. Fifth Conference on Carbon*, Pergamon, Oxford, UK **1962**, p. 73.
- [7] A. Nagashima, K. Nuka, H. Itoh, T. Ichinokawa, C. Oshima, S. Otani, *Surf. Sci.* **1993**, 291, 93.
- [8] Y. Souzu, M. Tsukada, *Surf. Sci.* **1995**, 326, 42.
- [9] T. Aizawa, R. Souda, Y. Ishizawa, H. Hirano, T. Yamada, K. Tanaka, C. Oshima, *Surf. Sci.* **1990**, 237, 194.
- [10] C. Backes, A. M. Abdelkader, C. Alonso, A. Andrieux-Ledier, R. Arenal, J. Azpeitia, N. Balakrishnan, L. Banszerus, J. Barjon, R. Bartali, S. Bellani, C. Berger, R. Berger, M. M. B. Ortega, C. Bernard, P. H. Beton, A. Beyer, A. Bianco, P. Boggild, F. Bonaccorso, G. B. Barin, C. Botas, R. A. Bueno, D. Carriazo, A. Castellanos-Gomez, M. Christian, A. Ciesielski, T. Ciuk, M. T. Cole, J. Coleman, et al., *2D Mater.* **2020**, 7, 022001.
- [11] A. J. Mannix, B. Kiraly, M. C. Hersam, N. P. Guisinger, *Nat. Rev. Chem.* **2017**, 1, 0014.
- [12] R. Ye, J. M. Tour, *ACS Nano* **2019**, 13, 10872.
- [13] Ö. Güler, N. Bağcı, *J. Mater. Res. Technol.* **2020**, 9, 6808.
- [14] L. Lavagna, G. Meligrana, C. Gerbaldi, A. Tagliaferro, M. Bartoli, *Energies* **2020**, 13, 4867.
- [15] V. B. Mohan, K. Lau, D. Hui, D. Bhattacharyya, *Composites, Part B* **2018**, 142, 200.
- [16] A. K. Geim, K. S. Novoselov, *Nat. Mater.* **2007**, 6, 183.
- [17] A. Nag, A. Mitra, S. C. Mukhopadhyay, *Sens. Actuators, A* **2018**, 270, 177.
- [18] D. G. Papageorgiou, I. A. Kinloch, R. J. Young, *Prog. Mater. Sci.* **2017**, 90, 75.
- [19] M. J. Allen, V. C. Tung, R. B. Kaner, *Chem. Rev.* **2010**, 110, 132.
- [20] A. J. Pollard, C. A. Clifford, *J. Mater. Sci.* **2017**, 52, 13685.
- [21] C. A. Clifford, E. H. Martins Ferreira, T. Fujimoto, J. Herrmann, A. R. Hight Walker, D. Koltsov, C. Punckt, L. Ren, G. J. Smallwood, A. J. Pollard, *Nat. Rev. Phys.* **2021**, 3, 233.
- [22] A. Bianco, H.-M. Cheng, T. Enoki, Y. Gogotsi, R. H. Hurt, N. Koratkar, T. Kyotani, M. Monthieux, C. R. Park, J. M. D. Tascon, J. Zhang, *Carbon* **2013**, 65, 1.
- [23] N. Gupta, S. Walia, U. Mogera, G. U. Kulkarni, *J. Phys. Chem. Lett.* **2020**, 11, 2797.
- [24] S. Shallcross, S. Sharma, E. Kandelaki, O. A. Pankratov, *Phys. Rev. B* **2010**, 81, 165105.
- [25] K. S. Novoselov, A. K. Geim, S. V. Morozov, D. Jiang, M. I. Katsnelson, I. V. Grigorieva, S. V. Dubonos, A. A. Firsov, *Nature* **2005**, 438, 197.
- [26] K. Kim, S. Coh, L. Z. Tan, W. Regan, J. M. Yuk, E. Chatterjee, M. F. Crommie, M. L. Cohen, S. G. Louie, A. Zettl, *Phys. Rev. Lett.* **2012**, 108, 246103.
- [27] T. Barkan, *Nat. Nanotechnol.* **2019**, 14, 904.
- [28] A. Zurutuza, C. Marinelli, *Nat. Nanotechnol.* **2014**, 9, 730.
- [29] A. C. Ferrari, F. Bonaccorso, V. Fal'ko, K. S. Novoselov, S. Roche, P. Boggild, S. Borini, F. H. L. Koppens, V. Palermo, N. Pugno, J. A. Garrido, R. Sordan, A. Bianco, L. Ballerini, M. Prato, E. Lidorikis, J. Kivioja, C. Marinelli, T. Ryhänen, A. Morpurgo, J. N. Coleman, V. Nicolosi, L. Colombo, A. Fert, M. Garcia-Hernandez, A. Bachtold, G. F. Schneider, F. Guinea, C. Dekker, M. Barbone, et al., *Nanoscale* **2015**, 7, 4598.
- [30] D. X. Luong, K. V. Bets, W. A. Algozeeb, M. G. Stanford, C. Kittrell, W. Chen, R. V. Salvatierra, M. Ren, E. A. McHugh, P. A. Advincula, Z. Wang, M. Bhatt, H. Guo, V. Mancevski, R. Shahsavari, B. I. Yakobson, J. M. Tour, *Nature* **2020**, 577, 647.
- [31] K. M. Wyss, J. L. Beckham, W. Chen, D. X. Luong, P. Hundi, S. Raghuraman, R. Shahsavari, J. M. Tour, *Carbon* **2021**, 174, 430.
- [32] P. A. Advincula, D. X. Luong, W. Chen, S. Raghuraman, R. Shahsavari, J. M. Tour, *Carbon* **2021**, 178, 649.
- [33] M. G. Stanford, K. V. Bets, D. X. Luong, P. A. Advincula, W. Chen, J. T. Li, Z. Wang, E. A. McHugh, W. A. Algozeeb, B. I. Yakobson, J. M. Tour, *ACS Nano* **2020**, 14, 13691.

- [34] W. A. Algozeeb, P. E. Savas, D. X. Luong, W. Chen, C. Kittrell, M. Bhat, R. Shahsavari, J. M. Tour, *ACS Nano* **2020**, *14*, 15595.
- [35] K. M. Wyss, Z. Wang, L. B. Alemany, C. Kittrell, J. M. Tour, *ACS Nano* **2021**, *15*, 10542.
- [36] W. Chen, Z. Wang, K. V. Bets, D. X. Luong, M. Ren, M. G. Stanford, E. A. McHugh, W. A. Algozeeb, H. Guo, G. Gao, B. Deng, J. Chen, J. T. Li, W. T. Carsten, B. I. Yakobson, J. M. Tour, *ACS Nano* **2021**, *15*, 1282.
- [37] W. Chen, J. T. Li, Z. Wang, W. A. Algozeeb, D. X. Luong, C. Kittrell, E. A. McHugh, P. A. Advincula, K. M. Wyss, J. L. Beckham, M. G. Stanford, B. Jiang, J. M. Tour, *ACS Nano* **2021**, *15*, 11158.
- [38] S. Chen, L. Brown, M. Levendorf, W. Cai, S.-Y. Ju, J. Edgeworth, X. Li, C. W. Magnuson, A. Velamakanni, R. D. Piner, J. Kang, J. Park, R. S. Ruoff, *ACS Nano* **2011**, *5*, 1321.
- [39] M. Ren, J. Zhang, J. M. Tour, *Carbon* **2018**, *139*, 880.
- [40] Z. Xu, C. Gao, *Mater. Today* **2015**, *18*, 480.
- [41] X. Ling, L. Xie, Y. Fang, H. Xu, H. Zhang, J. Kong, M. S. Dresselhaus, J. Zhang, Z. Liu, *Nano Lett.* **2010**, *10*, 553.
- [42] F. Bonaccorso, Z. Sun, T. Hasan, A. C. Ferrari, *Nat. Photonics* **2010**, *4*, 611.
- [43] P. H. Presumido, A. Primo, V. J. P. Vilar, H. Garcia, *Chem. Eng. J.* **2021**, *413*, 127510.
- [44] X. Miao, S. Tongay, M. K. Petterson, K. Berke, A. G. Rinzier, B. R. Appleton, A. F. Hebard, *Nano Lett.* **2012**, *12*, 2745.
- [45] A. Scidà, S. Haque, E. Treossi, A. Robinson, S. Smerzi, S. Ravesi, S. Borini, V. Palermo, *Mater. Today* **2018**, *21*, 223.
- [46] A. A. Alazemi, A. D. Dysart, S. J. Shaffer, V. G. Pol, L.-E. Stacked, F. Sadeghi, *Carbon* **2017**, *123*, 7.
- [47] K. Lee, H. Lee, Y. Shin, Y. Yoon, D. Kim, H. Lee, *Nano Energy* **2016**, *26*, 746.
- [48] L. Ji, Z. Tan, T. Kuykendall, E. J. An, Y. Fu, V. Battaglia, Y. Zhang, *Energy Environ. Sci.* **2011**, *4*, 3611.
- [49] Y.-J. Wan, L.-C. Tang, D. Yan, L. Zhao, Y.-B. Li, L.-B. Wu, J.-X. Jiang, G.-Q. Lai, *Compos. Sci. Technol.* **2013**, *82*, 60.
- [50] J. M. Tour, *Chem. Mater.* **2014**, *26*, 163.
- [51] Y. Zhang, L. Zhang, C. Zhou, *Acc. Chem. Res.* **2013**, *46*, 2329.
- [52] L. Lin, H. Peng, Z. Liu, *Nat. Mater.* **2019**, *18*, 520.
- [53] W. Ren, H.-M. Cheng, *Nat. Nanotechnol.* **2014**, *9*, 726.
- [54] S. Milana, *Nat. Nanotechnol.* **2019**, *14*, 919.
- [55] X. Rui, Y. Geng, X. Sun, H. Hao, S. Xiao, *Resour. Conserv. Recycl.* **2021**, *173*, 105732.
- [56] H. Döschner, T. Reiss, *2D Mater.* **2021**, *8*, 022004.
- [57] Graphene, 2017-2027, Analysis from IDTechEx Consulting, **2017**.
- [58] K. Yan, H. Peng, Y. Zhou, H. Li, Z. Liu, *Nano Lett.* **2011**, *11*, 1106.
- [59] L. Li, M. Zhou, L. Jin, L. Liu, Y. Mo, X. Li, Z. Mo, Z. Liu, S. You, H. Zhu, *Front. Mater.* **2019**, *6*, 325.
- [60] Y. Xu, H. Cao, Y. Xue, B. Li, W. Cai, *Nanomaterials* **2018**, *8*, 942.
- [61] K. Parvez, S. Yang, X. Feng, K. Müllen, *Synth. Met.* **2015**, *210*, 123.
- [62] D. C. Marcano, D. V. Kosynkin, J. M. Berlin, A. Sinitskii, Z. Sun, A. Slesarev, L. B. Alemany, W. Lu, J. M. Tour, *ACS Nano* **2010**, *4*, 4806.
- [63] V. Agarwal, P. B. Zetterlund, *Chem. Eng. J.* **2021**, *405*, 127018.
- [64] Y. L. Zhong, Z. Tian, G. P. Simon, D. Li, *Mater. Today* **2015**, *18*, 73.
- [65] X. Zhou, F. Liang, *Curr. Med. Chem.* **2014**, *21*, 855.
- [66] Y. Hernandez, V. Nicolosi, M. Lotya, F. M. Blighe, Z. Sun, S. De, I. T. McGovern, B. Holland, M. Byrne, Y. K. Gun'ko, J. J. Boland, P. Niraj, G. Duesberg, S. Krishnamurthy, R. Goodhue, J. Hutchison, V. Scardaci, A. C. Ferrari, J. N. Coleman, *Nat. Nanotechnol.* **2008**, *3*, 563.
- [67] A. P. Kauling, A. T. Seefeldt, D. P. Pisoni, R. C. Pradeep, R. Bentini, R. V. B. Oliveira, K. S. Novoselov, A. H. Castro Neto, *Adv. Mater.* **2018**, *30*, 1803784.
- [68] S. Bae, H. Kim, Y. Lee, X. Xu, J.-S. Park, Y. Zheng, J. Balakrishnan, T. Lei, H. Ri Kim, Y. I. Song, Y.-J. Kim, K. S. Kim, B. Özyilmaz, J.-H. Ahn, B. H. Hong, S. Iijima, *Nat. Nanotechnol.* **2010**, *5*, 574.
- [69] Y. Zhu, H. Ji, H.-M. Cheng, R. S. Ruoff, *Natl. Sci. Rev.* **2018**, *5*, 90.
- [70] Product overview: Compound Semiconductors and 2D Nanomaterials : AIXTRON, https://www.aixtron.com/en/products/AIX%20G5%2B%20C_p38 (accessed: August 2021).
- [71] J. Lin, Z. Peng, Y. Liu, F. Ruiz-Zepeda, R. Ye, E. L. G. Samuel, M. J. Yacaman, B. I. Yakobson, J. M. Tour, *Nat. Commun.* **2014**, *5*, 5714.
- [72] ViralWall Air Purifier for Social Distancing, LIGC App, <https://ligc-viralwall.com/> (accessed: August 2021).
- [73] R. Ye, D. K. James, J. M. Tour, *Acc. Chem. Res.* **2018**, *51*, 1609.
- [74] R. Ye, D. K. James, J. M. Tour, *Adv. Mater.* **2019**, *31*, 1803621.
- [75] J. T. Li, M. G. Stanford, W. Chen, S. E. Presutti, J. M. Tour, *ACS Nano* **2020**, *14*, 7911.
- [76] J. L. Beckham, J. T. Li, M. G. Stanford, W. Chen, E. A. McHugh, P. A. Advincula, K. M. Wyss, Y. Chyan, W. L. Boldman, P. D. Rack, J. M. Tour, *ACS Nano* **2021**, *15*, 8976.
- [77] Cell Phones, Sporting Goods, and Soon, Cars: Ford Innovates with "Miracle" Material, Powerful Graphene for Vehicle Parts, Ford Media Center, <https://media.ford.com/content/fordmedia/fna/us/en/news/2018/10/09/ford-innovates-with-miracle-material-powerful-graphene-for-vehicle-parts.html> (accessed: August 2021).
- [78] Real Graphene USA, <https://realgrapheneusa.com/> (accessed: August 2021).
- [79] Graphene Manufacturing Group, <https://graphenemg.com/> (accessed: August 2021).
- [80] Guangzhou Automobile Group Motor Co., Ltd., <https://www.gac-motor.com/en/media/newsdetail/id/166.html> (accessed: August 2021).
- [81] Chongqing Graphene Technology Corporation, Ltd., <http://cqmx.com/> (accessed: August 2021).
- [82] Grahope New Materials Technologies Corporation, <http://www.grahope.com/> (accessed: August 2021).
- [83] Elon Musk May Use "Wonder Material" Graphene To Push Tesla Performance To The Next Level, <https://www.businessinsider.com/elon-musk-may-use-graphene-tesla-2014-8> (accessed: August 2021).
- [84] Samsung Develops Battery Material with 5x Faster Charging Speed, <https://news.samsung.com/global/samsung-develops-battery-material-with-5x-faster-charging-speed> (accessed: August 2021).
- [85] DuPont Printed Electronic Materials, <https://www.dupont.com/electronic-materials/printed-electronics.html> (accessed: August 2021).
- [86] M. Cossutta, J. McKechnie, S. J. Pickering, *Green Chem.* **2017**, *19*, 5874.
- [87] E. S. Polsen, D. Q. McNerny, B. Viswanath, S. W. Pattinson, A. J. Hart, *Sci. Rep.* **2015**, *5*, 10257.
- [88] B. Deng, Z. Xin, R. Xue, S. Zhang, X. Xu, J. Gao, J. Tang, Y. Qi, Y. Wang, Y. Zhao, L. Sun, H. Wang, K. Liu, M. H. Rummeli, L.-T. Weng, Z. Luo, L. Tong, X. Zhang, C. Xie, Z. Liu, H. Peng, *Sci. Bull.* **2019**, *64*, 659.
- [89] K. R. Paton, E. Varra, C. Backes, R. J. Smith, U. Khan, A. O'Neill, C. Boland, M. Lotya, O. M. Istrate, P. King, T. Higgins, S. Barwich, P. May, P. Puczkarski, I. Ahmed, M. Moebius, H. Pettersson, E. Long, J. Coelho, S. E. O'Brien, E. K. McGuire, B. M. Sanchez, G. S. Duesberg, N. McEvoy, T. J. Pennycook, C. Downing, A. Crossley, V. Nicolosi, J. N. Coleman, *Nat. Mater.* **2014**, *13*, 624.
- [90] X. Zhang, L. Wang, Q. Lu, D. L. Kaplan, *ACS Appl. Mater. Interfaces* **2018**, *10*, 22924.
- [91] J. Stafford, N. Uzo, U. Farooq, S. Favero, S. Wang, H.-H. Chen, A. L'Hermite, C. Petit, O. Matar, *2D Mater.* **2021**, *8*, 025029.
- [92] S. Yousef, A. Mohamed, M. Tatarants, *Tribol. Int.* **2018**, *121*, 54.
- [93] H. Gao, K. Zhu, G. Hu, C. Xue, *Chem. Eng. J.* **2017**, *308*, 872.
- [94] M. K. Bayazit, L. Xiong, C. Jiang, S. J. A. Moniz, E. White, M. S. P. Shaffer, J. Tang, *ACS Appl. Mater. Interfaces* **2021**, *13*, 28600.
- [95] Y. Zhang, Y. Xu, *Adv. Funct. Mater.* **2019**, *29*, 1902171.

- [96] M. H. Chakrabarti, N. S. A. Manan, N. P. Brandon, R. C. Maher, F. S. Mjalli, I. M. AlNashef, S. A. Hajimolana, M. A. Hashim, M. A. Hussain, D. Nir, *Chem. Eng. J.* **2015**, 274, 213.
- [97] P. C. Shi, J. P. Guo, X. Liang, S. Cheng, H. Zheng, Y. Wang, C. H. Chen, H. F. Xiang, *Carbon* **2018**, 126, 507.
- [98] A. Islam, B. Mukherjee, K. K. Pandey, A. K. Keshri, *ACS Nano* **2021**, 15, 1775.
- [99] X. Wu, Y. Liu, H. Yang, Z. Shi, *RSC Adv.* **2016**, 6, 93119.
- [100] P. R. Kidambi, D. D. Mariappan, N. T. Dee, A. Vyatsikh, S. Zhang, R. Karnik, A. J. Hart, *ACS Appl. Mater. Interfaces* **2018**, 10, 10369.
- [101] T. Wu, X. Zhang, Q. Yuan, J. Xue, G. Lu, Z. Liu, H. Wang, H. Wang, F. Ding, Q. Yu, X. Xie, M. Jiang, *Nat. Mater.* **2016**, 15, 43.
- [102] Z. Yan, Y. Liu, L. Ju, Z. Peng, J. Lin, G. Wang, H. Zhou, C. Xiang, E. L. G. Samuel, C. Kittrell, V. I. Artyukhov, F. Wang, B. I. Yakobson, J. M. Tour, *Angew. Chem., Int. Ed.* **2014**, 53, 1565.
- [103] Z. Yan, J. Lin, Z. Peng, Z. Sun, Y. Zhu, L. Li, C. Xiang, E. L. Samuel, C. Kittrell, J. M. Tour, *ACS Nano* **2012**, 6, 9110.
- [104] I. V. Vlassiok, Y. Stehle, P. R. Pudasaini, R. R. Unocic, P. D. Rack, A. P. Baddorf, I. N. Ivanov, N. V. Lavrik, F. List, N. Gupta, K. V. Bets, B. I. Yakobson, S. N. Smirnov, *Nat. Mater.* **2018**, 17, 318.
- [105] J. Lee, S. Lee, H. K. Yu, *Coatings* **2017**, 7, 218.
- [106] M. Hempel, A.-Y. Lu, F. Hui, T. Kpulum, M. Lanza, G. Harris, T. Palacios, J. Kong, *Nanoscale* **2018**, 10, 5522.
- [107] M. M. Tavakoli, G. Azzellino, M. Hempel, A.-Y. Lu, F. J. Martin-Martinez, J. Zhao, J. Yeo, T. Palacios, M. J. Buehler, J. Kong, *Adv. Funct. Mater.* **2020**, 30, 2001924.
- [108] B.-J. Park, J.-S. Choi, J.-H. Eom, H. Ha, H. Y. Kim, S. Lee, H. Shin, S.-G. Yoon, *ACS Nano* **2018**, 12, 2008.
- [109] N. Wei, L. Yu, Z. Sun, Y. Song, M. Wang, Z. Tian, Y. Xia, J. Cai, Y. Li, L. Zhao, Q. Li, M. H. Rummeli, J. Sun, Z. Liu, *ACS Nano* **2019**, 13, 7517.
- [110] C. Li, X. Zhang, K. Wang, X. Sun, G. Liu, J. Li, H. Tian, J. Li, Y. Ma, *Adv. Mater.* **2017**, 29, 1604690.
- [111] C. Melero, R. Rincón, J. Muñoz, G. Zhang, S. Sun, A. Perez, O. Royuela, C. González-Gago, M. D. Calzada, *Plasma Phys. Controlled Fusion* **2017**, 60, 014009.
- [112] A. Nepal, G. P. Singh, B. N. Flanders, C. M. Sorensen, *Nanotechnology* **2013**, 24, 245602.
- [113] J. Jang, M. Son, S. Chung, K. Kim, C. Cho, B. H. Lee, M.-H. Ham, *Sci. Rep.* **2015**, 5, 17955.
- [114] J. Fujita, T. Hiyama, A. Hirukawa, T. Kondo, J. Nakamura, S. Ito, R. Araki, Y. Ito, M. Takeguchi, W. W. Pai, *Sci. Rep.* **2017**, 7, 12371.
- [115] S. Zhang, S.-F. Jiang, B.-C. Huang, X.-C. Shen, W.-J. Chen, T.-P. Zhou, H.-Y. Cheng, B.-H. Cheng, C.-Z. Wu, W.-W. Li, H. Jiang, H.-Q. Yu, *Nat. Sustainability* **2020**, 3, 753.
- [116] S. Pei, Q. Wei, K. Huang, H.-M. Cheng, W. Ren, *Nat. Commun.* **2018**, 9, 145.
- [117] B. Meka Chufa, B. Abdisa Gonfa, T. Yohannes Anshebo, G. Adam Workneh, *Adv. Condens. Matter Phys.* **2021**, 2021, e6681710.
- [118] F. G. Torres, O. P. Troncoso, L. Rodriguez, G. E. De-la-Torre, *Sustainable Mater. Technol.* **2021**, 29, e00310.
- [119] K. K. H. De Silva, H.-H. Huang, R. K. Joshi, M. Yoshimura, *Carbon* **2017**, 119, 190.
- [120] T. H. Im, D. Y. Park, H. K. Lee, J. H. Park, C. K. Jeong, D. J. Joe, K. J. Lee, *Part. Part. Syst. Character.* **2017**, 34, 1600429.
- [121] D. W. Chang, H.-J. Choi, I.-Y. Jeon, J.-M. Seo, L. Dai, J.-B. Baek, *Carbon* **2014**, 77, 501.
- [122] T. Homola, J. Pospíšil, R. Krumpolec, P. Souček, P. Dzik, M. Weiter, M. Černák, *ChemSusChem* **2018**, 11, 941.
- [123] R. Jakhar, J. E. Yap, R. Joshi, *Carbon* **2020**, 170, 277.
- [124] L. Dong, Z. Chen, X. Zhao, J. Ma, S. Lin, M. Li, Y. Bao, L. Chu, K. Leng, H. Lu, K. P. Loh, *Nat. Commun.* **2018**, 9, 76.
- [125] S. Zhao, S. Xie, Z. Zhao, J. Zhang, L. Li, Z. Xin, *ACS Sustainable Chem. Eng.* **2018**, 6, 7652.
- [126] S.-J. Yuan, B. Dong, X.-H. Dai, *Appl. Surf. Sci.* **2021**, 562, 150203.
- [127] J.-I. Fujita, S. Nakazawa, T. Ichihashi, M. Ishida, T. Kaito, S. Matsui, *Microelectron. Eng.* **2007**, 84, 1507.
- [128] R. K. Murakami, V. Villas-Boas, *Mater. Res.* **1999**, 2, 67.
- [129] M. Cologna, B. Rashkova, R. Raj, *J. Am. Ceram. Soc.* **2010**, 93, 3556.
- [130] C. E. J. Dancer, *Mater. Res. Express* **2016**, 3, 102001.
- [131] R. Raj, *J. Eur. Ceram. Soc.* **2012**, 32, 2293.
- [132] T. B. Holland, U. Anselmi-Tamburini, D. V. Quach, T. B. Tran, A. K. Mukherjee, *J. Eur. Ceram. Soc.* **2012**, 32, 3667.
- [133] I. V. Okulov, I. V. Soldatov, M. F. Sarmanova, I. Kaban, T. Gemming, K. Edström, J. Eckert, *Nat. Commun.* **2015**, 6, 7932.
- [134] O. Guillon, J. Gonzalez-Julian, B. Dargatz, T. Kessel, G. Schiering, J. Räthel, M. Herrmann, *Adv. Eng. Mater.* **2014**, 16, 830.
- [135] J. Perelaer, R. Jani, M. Grouchko, A. Kamyshtny, S. Magdassi, U. S. Schubert, *Adv. Mater.* **2012**, 24, 3993.
- [136] K. S. N. Vikrant, H. Wang, A. Jana, H. Wang, R. E. García, *npj Comput. Mater.* **2020**, 6, 98.
- [137] E. A. Olevsky, S. M. Roling, A. L. Maximenko, *Sci. Rep.* **2016**, 6, 33408.
- [138] Y. Yao, K. K. Fu, S. Zhu, J. Dai, Y. Wang, G. Pastel, Y. Chen, T. Li, C. Wang, T. Li, L. Hu, *Nano Lett.* **2016**, 16, 7282.
- [139] H. Xie, K. Fu, C. Yang, Y. Yao, J. Rao, Y. Zhou, B. Liu, D. Kirsch, L. Hu, *Small Methods* **2018**, 2, 1700371.
- [140] Y. J. Kwon, Y. Kwon, H. S. Park, J. U. Lee, *Adv. Mater. Interfaces* **2019**, 6, 1900095.
- [141] C. Knieke, A. Berger, M. Voigt, R. N. K. Taylor, J. Röhr, W. Peukert, *Carbon* **2010**, 48, 3196.
- [142] X. Geng, Y. Guo, D. Li, W. Li, C. Zhu, X. Wei, M. Chen, S. Gao, S. Qiu, Y. Gong, L. Wu, M. Long, M. Sun, G. Pan, L. Liu, *Sci. Rep.* **2013**, 3, 1134.
- [143] W. Lu, S. Liu, X. Qin, L. Wang, J. Tian, Y. Luo, A. M. Asiri, A. O. Al-Youbi, X. Sun, *J. Mater. Chem.* **2012**, 22, 8775.
- [144] A. Merlen, J. G. Buijnsters, C. Pardauna, *Coatings* **2017**, 7, 153.
- [145] L. M. Malard, M. A. Pimenta, G. Dresselhaus, M. S. Dresselhaus, *Phys. Rep.* **2009**, 473, 51.
- [146] A. C. Ferrari, D. M. Basko, *Nat. Nanotechnol.* **2013**, 8, 235.
- [147] J.-B. Wu, M.-L. Lin, X. Cong, H.-N. Liu, P.-H. Tan, *Chem. Soc. Rev.* **2018**, 47, 1822.
- [148] H. Kato, N. Itagaki, H. J. Im, *Carbon* **2019**, 141, 76.
- [149] A. C. Ferrari, *Solid State Commun.* **2007**, 143, 47.
- [150] D. R. Lenski, M. S. Fuhrer, *J. Appl. Phys.* **2011**, 110, 013720.
- [151] J. A. Garlow, L. K. Barrett, L. Wu, K. Kisslinger, Y. Zhu, J. F. Pulecio, *Sci. Rep.* **2016**, 6, 19804.
- [152] A. Jorio, L. G. Cançado, *Solid State Commun.* **2013**, 175, 3.
- [153] M. Yi, Z. Shen, *J. Mater. Chem. A* **2015**, 3, 11700.
- [154] C.-M. Seah, S.-P. Chai, A. R. Mohamed, *Carbon* **2014**, 70, 1.
- [155] A. E. Balfour, H. L. Riley, *J. Chem. Soc.* **1935**, 1723.
- [156] S. Wang, K. Komvopoulos, *Thin Solid Films* **2020**, 713, 138247.
- [157] R. E. Franklin, J. T. Randall, *Proc. R. Soc. London, Ser. A* **1951**, 209, 196.
- [158] J. Y. Huang, S. Chen, Z. F. Ren, G. Chen, M. S. Dresselhaus, *Nano Lett.* **2006**, 6, 1699.
- [159] A. Gao, C. Su, S. Luo, Y. Tong, L. Xu, *J. Phys. Chem. Solids* **2011**, 72, 1159.
- [160] Y. Sun, A. G. Kvashnin, P. B. Sorokin, B. I. Yakobson, W. E. Billups, *J. Phys. Chem. Lett.* **2014**, 5, 1924.
- [161] P. V. Bakharev, M. Huang, M. Saxena, S. W. Lee, S. H. Joo, S. O. Park, J. Dong, D. C. Camacho-Mojica, S. Jin, Y. Kwon, M. Biswal, F. Ding, S. K. Kwak, Z. Lee, R. S. Ruoff, *Nat. Nanotechnol.* **2020**, 15, 59.
- [162] S. Gupta, J. Narayan, *Mater. Res. Lett.* **2020**, 8, 408.
- [163] R. Ye, X. Han, D. V. Kosynkin, Y. Li, C. Zhang, B. Jiang, A. A. Martí, J. M. Tour, *ACS Nano* **2018**, 12, 1083.

- [164] S. Manzeli, D. Ovchinnikov, D. Pasquier, O. V. Yazyev, A. Kis, *Nat. Rev. Mater.* **2017**, 2, 17033.
[165] G.-B. Liu, D. Xiao, Y. Yao, X. Xu, W. Yao, *Chem. Soc. Rev.* **2015**, 44, 2643.

- [166] M. Bosi, *RSC Adv.* **2015**, 5, 75500.
[167] D. Voiry, A. Mohite, M. Chhowalla, *Chem. Soc. Rev.* **2015**, 44, 2702.



Kevin M. Wyss received his B.S. degree in chemistry from Auburn University in Auburn, Alabama, USA under the guidance of Prof. Anne Gorden and the mentorship of Prof. Richard Kemp. His current research at Rice University focuses on flash Joule heating assisted upcycling of waste materials into graphene and other high-value products, as well as their practical and sustainable application in composites, energy-storage devices, and electrocatalysts.



Duy Xuan Luong received his B.S. in nanotechnology from Chiba University in Chiba, Japan, and completed his Ph.D. training at Rice University in the Applied Physics Program under the guidance of Prof. James Tour where he invented the synthetic flash Joule heating process to make graphene and he also studied laser-induced graphene. He continued his work as a postdoctoral researcher and then joined Universal Matter Inc. as a Senior Research Scientist in June 2021.



James M. Tour is a synthetic organic chemist, and he is presently the T. T. and W. F. Chao Professor of Chemistry, Professor of Computer Science, and Professor of Materials Science and NanoEngineering at Rice University. He conducts research across a broad range of nanotechnology areas that are energy, materials, environment, and medically related.